4.1. CdS synthesized by a microwave plasma technique

X-ray diffraction (XRD) patterns can provide an effective method for determining the phase and crystallite size of the CdS samples. The XRD patterns of CdS microstructure synthesized by microwave plasma technique are shown in Figure 4.1(a) and (b)
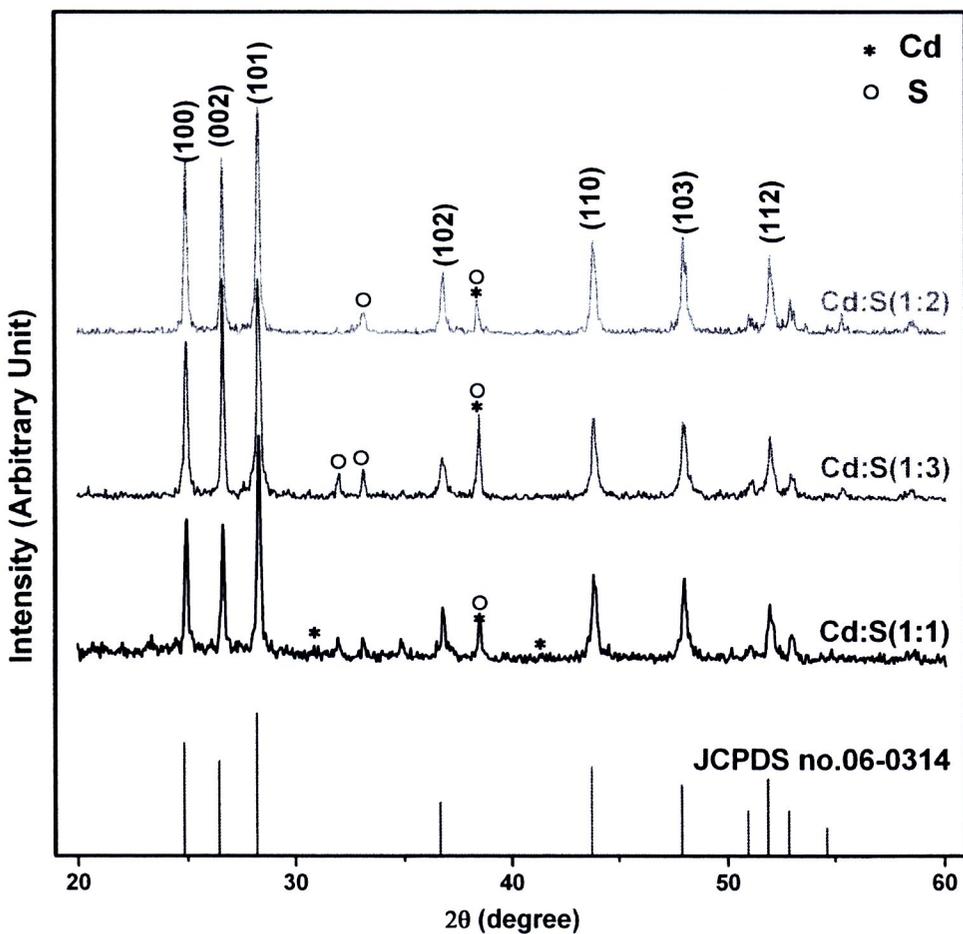

Figure 4.1 (a) XRD patterns of CdS synthesized using power 900W and different Cd:S molar ratios for 20 min

All the peaks can be indexed with the standard JCPDS data 06-0314 (a = b = 4.1360 Å and c = 6.7130 Å) [110] as hexagonal wurtzite crystal structure due to the presence of (100), (002), (101), (102), (110), (103), (200), (112) and (201) diffraction planes. At 20 min and 1:1 molar ratio of Cd:S, the product contains some Cd and S impurities. It showed that some S evaporated, leaving Cd as residue. Upon increasing S to be at 1:3 molar ratio, the product was CdS with significant Cd and S as impurities. Thus 1:2 molar ratio of Cd:S shown in Figure 4.1 (b) was used.
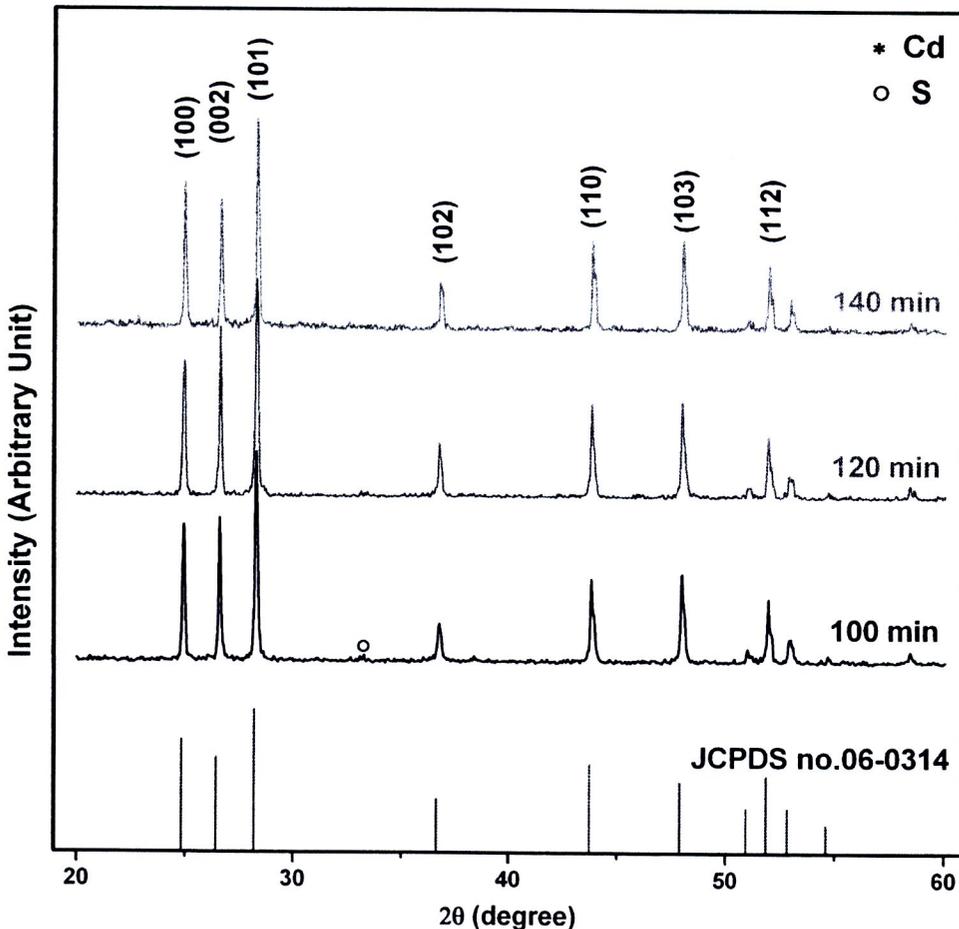

Figure4.1 (b) XRD patterns of CdS synthesized using power 900W, 1:2 molar ratio of Cd:S and different lengths of time for heating by microwave plasma.

At this stage, only little impurities were still left in the product. By increasing the lengths of time in a series of steps, the impurities became lessened, and the CdS peaks were higher. Until at 120 min and 140 min, the chemical reaction of Cd and S was complete, and only hexagonal CdS was produced as the main product, pure CdS crystals were synthesized.

The shape of XRD patterns indicated good crystallization of CdS. The strongest intensity peak of diffraction patterns at plane (101) are 2θ=28.326, 28.328 and 28.336 degrees, respectively. Lattice parameters of CdS were calculated using plane-spacing equation for hexagonal structure and Bragg's law for diffraction. They are a = b = 4.1243 Å and c = 6.7340 Å for 100 min (Table 4.1), a = b = 4.1243 Å and c = 6.7340 Å for 120 min (Table 4.2) and a = b = 4.1233 Å and c = 6.7340 Å for 140 min (Table 4.3), which are very close to the JCPDS standard value. XRD pattern is shown the good crystalline character for CdS samples. XRD patterns of Figure 4.1 indicates that, with increasing the length of time from 20 min to 140 min, there are effective change in XRD peak intensity and purity of corresponding CdS products.

Table 4.1 Calculated lattice parameter of CdS from the experiment (molar ratio of Cd:S=1:2, 100 min), comparing with the JCPDS file (Reference code: 06-0314 [78] for CdS)

Plane	2θ (Exp.)	2θ (JCPDS)	d-spacing JCPDS A°	Lattice parameter (Exp.) A°	Lattice parameter (JCPDS) A°
(100)	24.94	24.83	3.583	4.1373	4.136
(002)	26.62	26.45	3.367	-	4.136
(101)	28.32	28.22	3.160	-	4.136
(102)	36.76	36.65	2.450	-	4.136
(110)	43.80	43.74	2.068	4.1360	4.136
(103)	47.96	47.89	1.898	-	4.136
(200)	51.09	50.95	1.791	4.1361	4.136
(112)	52.05	51.88	1.761	-	4.136
(201)	53.21	52.85	1.731	-	4.136
			Average.	a=4.1364	a=4.136
				c=6.7340	c=6.7130

Table 4.2 Calculated lattice parameter of CdS from the experiment (molar ratio of Cd:S=1:2, 120 min), comparing with the JCPDS file (Reference code: 06-0314 [78] for CdS)

Plane	2θ (Exp.)	2θ (JCPDS)	d-spacing JCPDS A°	Lattice parameter (Exp.) A°	Lattice parameter (JCPDS) A°
(100)	24.92	24.83	3.583	4.1225	4.136
(002)	26.60	26.45	3.367	-	4.136
(101)	28.32	28.22	3.160	-	4.136
(102)	36.72	36.65	2.450	-	4.136
(110)	43.80	43.74	2.068	4.1304	4.136
(103)	47.96	47.89	1.898	-	4.136
(200)	51.16	50.95	1.791	4.1200	4.136
(112)	51.92	51.88	1.761	-	4.136
(201)	52.92	52.85	1.731	-	4.136
			Average.	a=4.1243	a=4.136
				c=6.7340	c=6.7130

Table 4.3 Calculated lattice parameter of CdS from the experiment (molar ratio of Cd:S=1:2, 140 min), comparing with the JCPDS file (Reference code: 06-0314 [78] for CdS)

Plane	2θ (Exp.)	2θ (JCPDS)	d-spacing JCPDS A°	Lattice parameter (Exp.) A°	Lattice parameter (JCPDS) A°
(100)	24.92	24.83	3.583	4.1225	4.136
(002)	26.60	26.45	3.367	-	4.136
(101)	28.32	28.22	3.160	-	4.136
(102)	36.72	36.65	2.450	-	4.136
(110)	43.80	43.74	2.068	4.1304	4.136
(103)	48.00	47.89	1.898	-	4.136
(200)	51.20	50.95	1.791	4.1170	4.136
(112)	51.96	51.88	1.761	-	4.136
(201)	52.96	52.85	1.731	-	4.136
			Average.	a=4.1233	a=4.136
				c=6.7340	c=6.7130

Table 4.4 The 2θ diffraction angles and intensities of the JCPDS no. 06-0314 [78] and for the 1:2 molar ratio of Cd:S and 100 min product obtained from the experiment and simulation.

Plane (hkl)	JCPDS (no. 06-0314)		Experimental		Simulation	
	2θ (deg.)	Intensity (%)	2θ (deg.)	Intensity (%)	2θ (deg.)	Intensity (%)
(100)	24.83	75	24.94	76.03	24.84	26.1
(002)	26.45	60	26.62	84.75	26.53	18.8
(101)	28.22	100	28.32	100	28.22	100
(102)	36.65	25	36.76	20.30	36.66	11.5
(110)	43.74	55	43.81	49.36	43.74	20.3
(103)	47.89	40	47.96	38.65	47.89	9.6
(200)	50.95	18	51.20	12.02	50.95	3
(112)	51.88	45	51.96	3.22	51.89	15.2
(201)	52.85	18	52.97	7.77	52.86	14.5

Table 4.5 The 2θ diffraction angles and intensities of the JCPDS no. 06-0314 [78] and for the 1:2 molar ratio of Cd:S and 120 min product obtained from the experiment and simulation.

Plane (hkl)	JCPDS (no. 06-0314)		Experimental		Simulation	
	2θ (deg.)	Intensity (%)	2θ (deg.)	Intensity (%)	2θ (deg.)	Intensity (%)
(100)	24.83	75	24.92	62.03	24.84	26.1
(002)	26.45	60	26.60	80.64	26.53	18.8
(101)	28.22	100	28.32	100	28.22	100
(102)	36.65	25	36.72	20.18	36.66	11.5
(110)	43.74	55	43.80	37.38	43.74	20.3
(103)	47.89	40	47.96	46.30	47.89	9.6
(200)	50.95	18	51.16	28.30	50.95	3
(112)	51.88	45	51.92	9.05	51.89	15.2
(201)	52.85	18	52.92	7.46	52.86	14.5

Table 4.6 The 2θ diffraction angles and intensities of the JCPDS no. 06-0314 [78] and for the 1:2 molar ratio of Cd:S and 140 min product obtained from the experiment and simulation.

Plane (hkl)	JCPDS (no. 06-0314)		Experimental		Simulation	
	2θ (deg.)	Intensity (%)	2θ (deg.)	Intensity (%)	2θ (deg.)	Intensity (%)
(100)	24.83	75	24.92	62.56	24.84	26.1
(002)	26.45	60	26.60	56.41	26.53	18.8
(101)	28.22	100	28.32	100	28.22	100
(102)	36.65	25	36.72	18.53	36.66	11.5
(110)	43.74	55	43.80	46.35	43.74	20.3
(103)	47.89	40	48.00	39.80	47.89	9.6
(200)	50.95	18	51.20	34.02	50.95	3
(112)	51.88	45	51.96	10.22	51.89	15.2
(201)	52.85	18	52.96	5.85	52.86	14.5

To calculate the crystallinity percentage of 1:2 molar ratio for 20, 40, 60, 80, 100,120 and 140 min, take the intensity ratio of peaks (101) and (112) at 2θ values as show in Table 4.7, indicate when length of time for heating is long the crystallinity of product, at 140 min, close the standard value.

Table 4.7 Crystallinities percentage of 1:2 molar ratio for 100, 120, 140 min and standard values.

Condition	Intensity (%) of peak (101)	Intensity (%) of peak (112)	Intensity ratio (101)/(112)
100 min	100	3.22	31.06
120 min	100	9.05	11.05
140 min	100	10.22	9.78
JCPDS	100	45	2.22
Simulation	100	15.2	6.58

Crystallite size (D) of 1:2 molar ratio CdS for 100, 120 and 140 min products were calculated using (111) peak of XRD spectra and Scherrer's formula [9].

$$D = \frac{k\lambda}{\beta \cos\theta} \tag{4.1}$$

k is the geometric (shaped) factor which usually takes a value of 0.94 [45,82] λ is the wavelength of X-ray Cu K_α radiation (0.15406 nm), and β and θ are the full width at half the peak maximum in radians unit and Bragg's angle in degree unit of the (111) peak, respectively. The results of crystallite size (D) graphs and data analysis are shown in Figure 4.2 (a), (b) and Table 4.8. The calculated size of the 1:1 molar ratio CdS for 100, 120 and 140 min products are 69.376, 69.377 and 69.378 nm respectively.
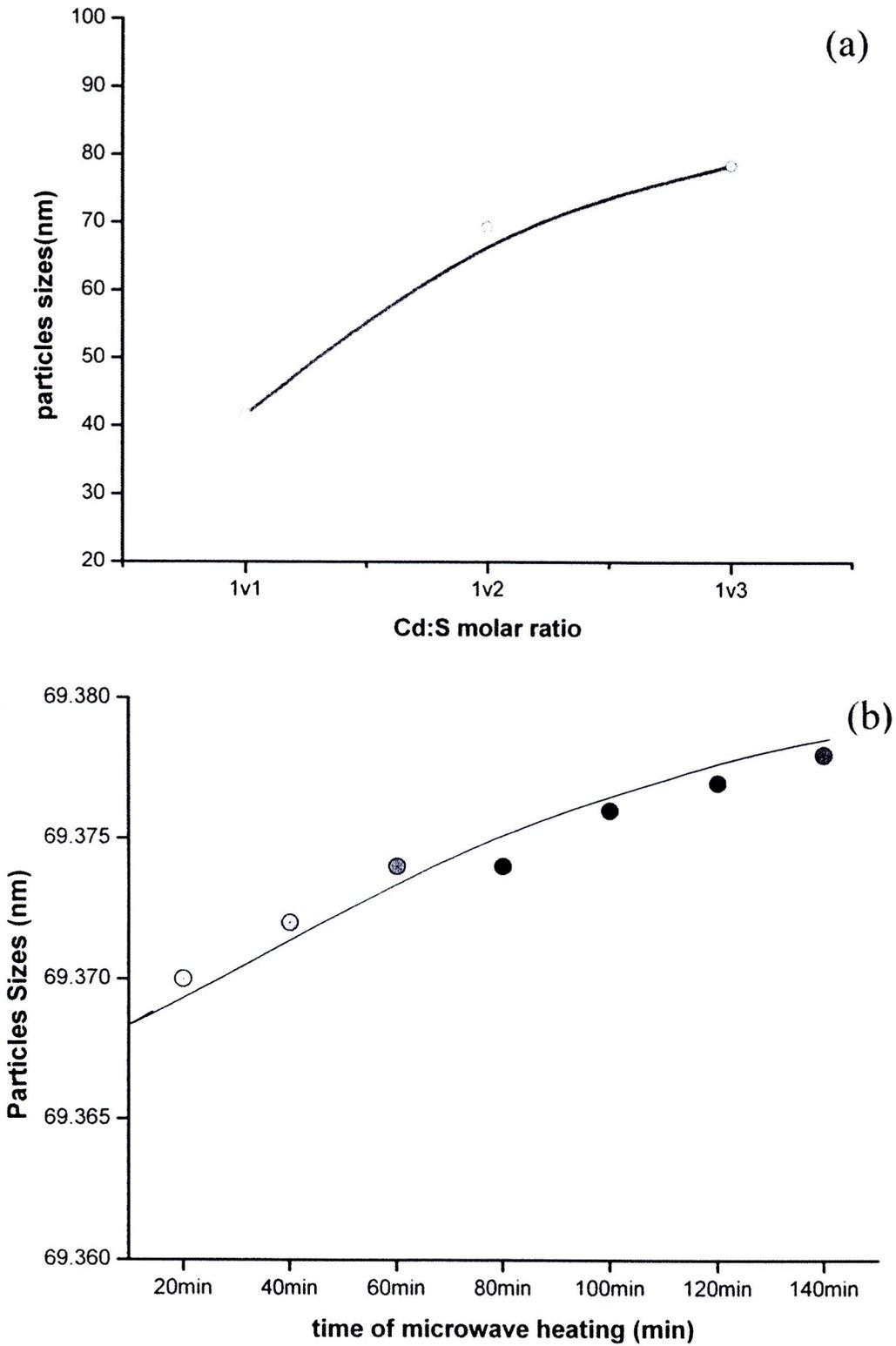
Figure 4.2 Particles Sizes of CdS synthesized using (a) different molar ratio at 20 min (b) different lengths of time for heating at 1:2 molar ratio.

Table 4.8 The crystallite size (D) of 1:2 molar ratio CdS for 100, 120 and 140 min products calculated from the scherrer's formula and the full width at half maximum (FWHM) of the XRD spectra

Experiment	Cd:S	2θ	FWHM	D (nm)
20 min	1:1	28.292	0.1968	41.630
20 min	1:3	28.412	0.1045	78.420
20 min	1:2	28.336	0.1181	69.378
40 min	1:2	28.298	0.1181	69.372
60 min	1:2	28.309	0.1181	69.374
80 min	1:2	28.309	0.1181	69.374
100 min	1:2	28.326	0.1181	69.376
120 min	1:2	28.328	0.1181	69.377
140 min	1:2	28.336	0.1181	69.378
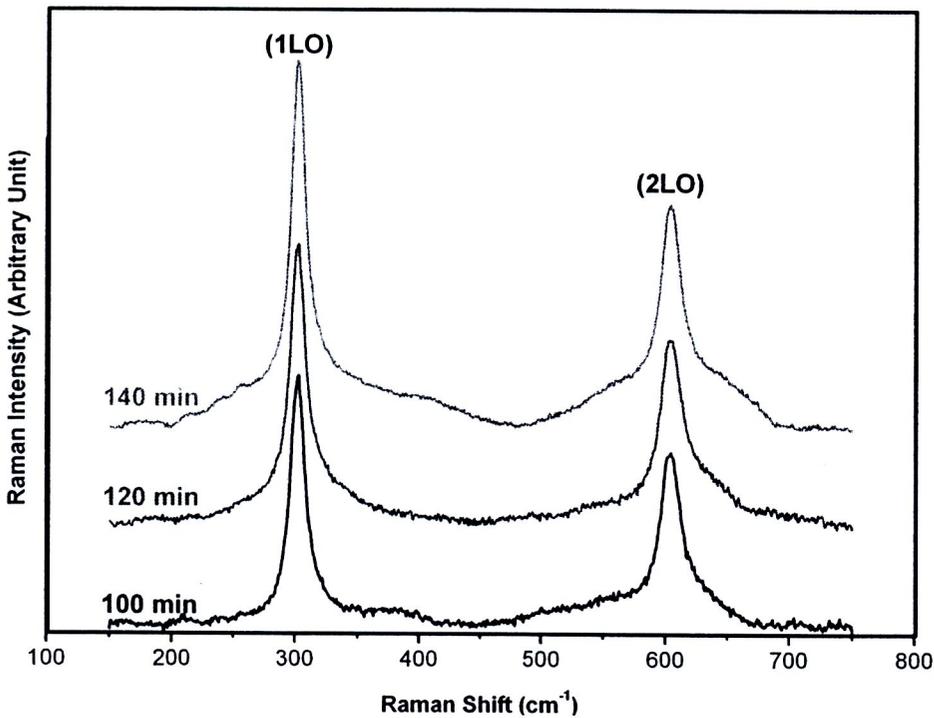
Figure 4.3 Raman spectra of 1:2 molar ratio CdS synthesized for 120 min and 140 min.

Figure 4.3, Raman spectra of 1:2 molar ratio CdS for 120 and 140 min were expected to show two longitudinal optical modes, the first harmonic (1LO) and second harmonic (2LO) modes at 303 and 605 cm^{-1},respectively. It should be noted that intensity of the first harmonic is stronger than that of the second. These results are in accordance with the previous reports [24]. These Raman shifts are good accordance with those obtained by Q. Zhang [23], who specified the 1LO and 2LO Raman shift of CdS nanostructure at 301.32, 603.56 cm^{-1} respectively.
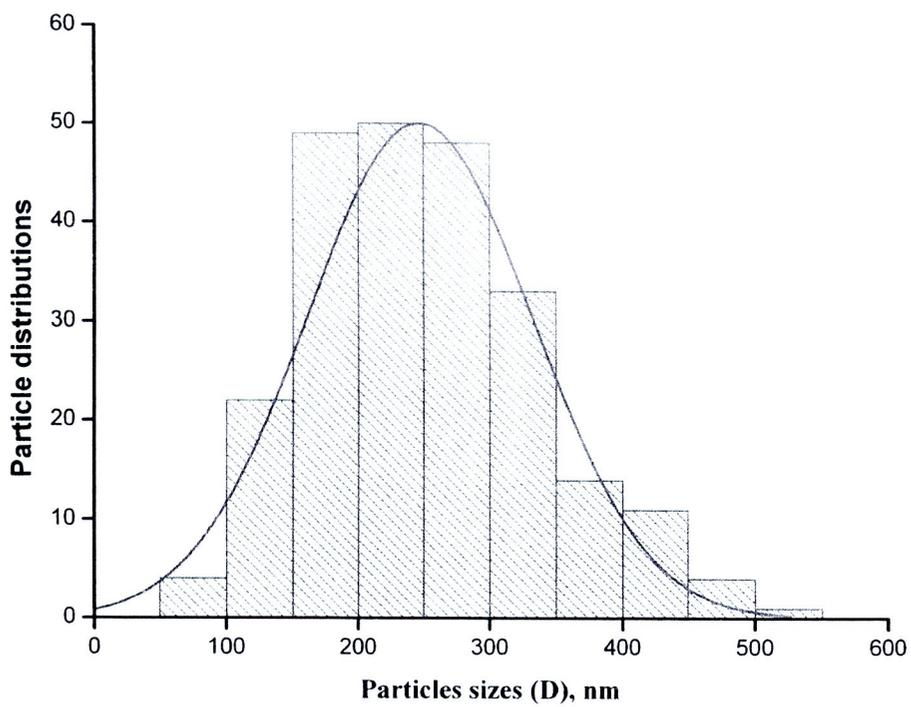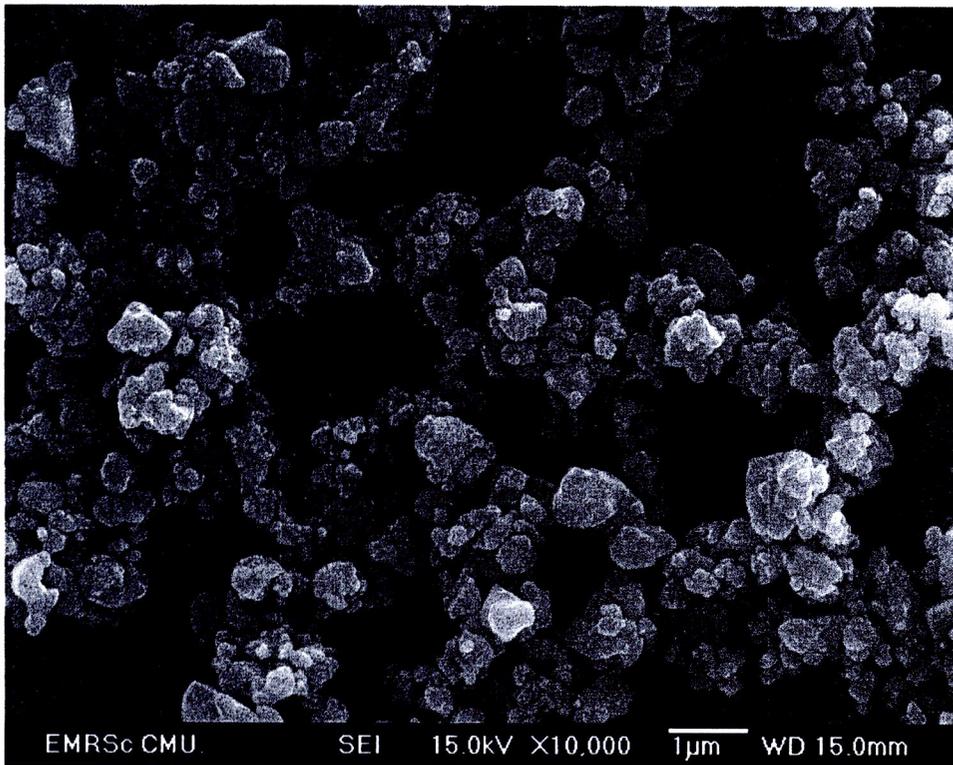
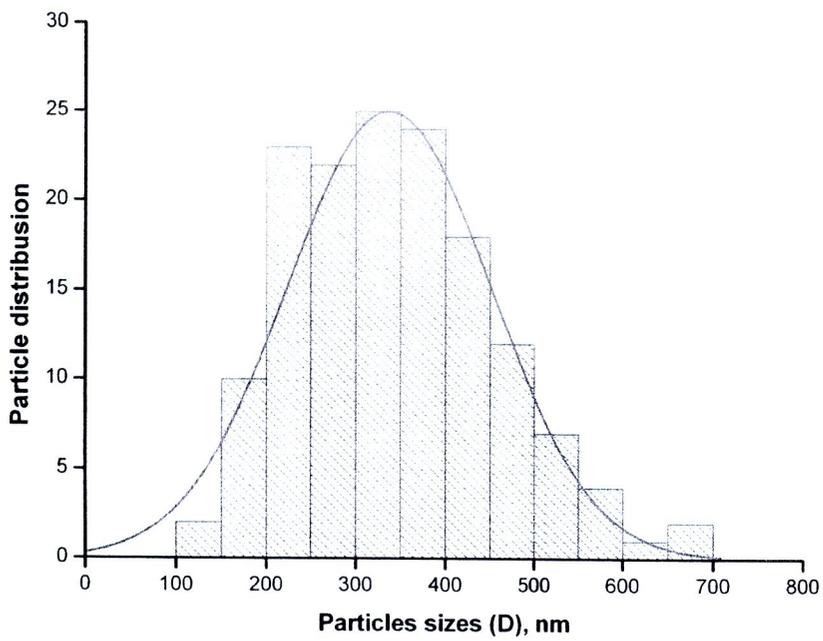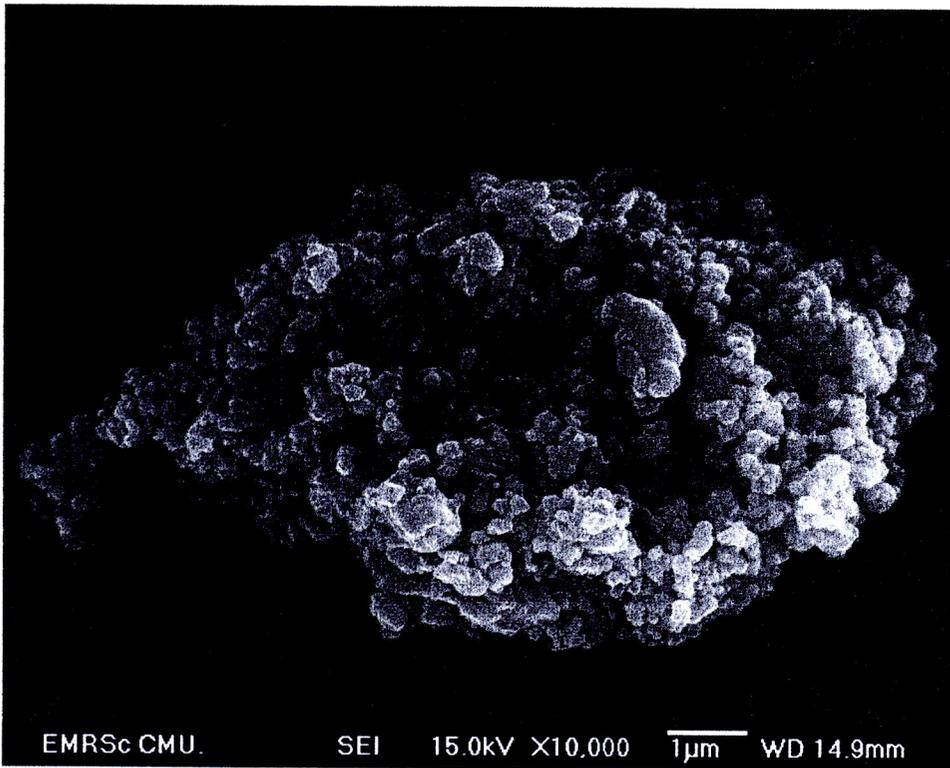Figure 4.4 SEM image and clusters sizes of 1:2 molar ratio CdS product for 120 min

Figure 4.5 SEM image and clusters sizes of 1:2 molar ratio CdS product for 140 min

SEM image and clusters size distribution of the products (Figure 4.4 - 4.5) show that morphologies of the products prepared at 1:2 molar ratio of Cd:S for 120 min and 140 min. Both 120 and 140 min compose of nano-sized particles in clusters and their packing densities are the highest. The average size of products 120, 140 min are around 246.48 ± 5.60 nm, 337.33 ± 9.31 nm respectively. Clusters sizes were increasing with length of time for heating that indicate the products have been thermal expansion. The value of average size is different, calculated using the scherrer's equation, because both condition produced different size of clusters and average size of particles are measured on the surface of each clusters. Therefore the calculated crystallite size of particle from Scherrer's equation using the full width at half maximum is the average values of total particles. The average size of SEM image does not cover total particles because measured only surface of clusters.

Photoluminescence or photoemission of CdS crystals (Figure 4.6) recorded using 210 nm excitation wavelength at room temperature. The emission was represented as broad peaks with the maximum emission at about 537 nm (2.31 eV) in the green-yellow region, and is in accordance with the other reports [27]. This emission may have different values, controlled by structural disorder and defects. It was blue-shift upon doping with Zn^{2+}. This behavior was the opposite, when the material was doped with Cu^{2+} [28]. Sometimes trap levels may reside in the band gap during processing, which result to the red-shift behavior.
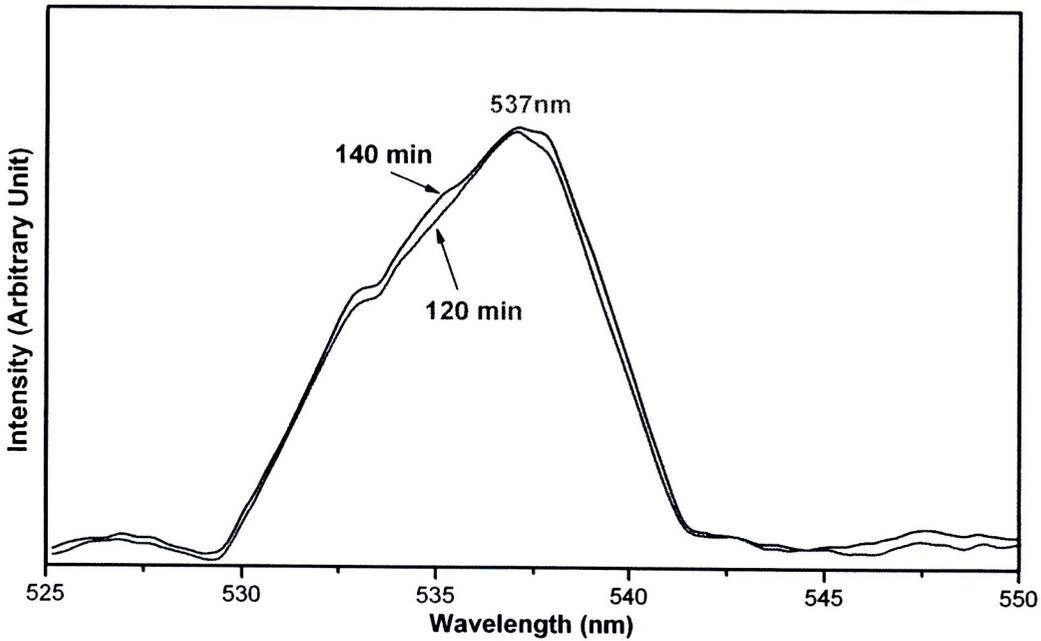
Figure 4.6 Photoluminescence of CdS produced under the 1:2 molar ratio of CdS condition

The absorption coefficient of CdS synthesized was calculated using the transmittance (T) value and thickness d using the relation:

$$\alpha = -\frac{\ln(T)}{d} \qquad (4.2)$$

The absorption coefficient α can be expressed by Urbach relation as show in equation (2.27) for direct gap CdS

$$(\alpha h v)^2 = A^*\left(hv - E_g\right) \qquad (4.3)$$

UV-vis absorbance of CdS was recorded. The direct energy gap (E_g) was determined by plotting $(\alpha hv)^2$ versus hv (Figure 4.7), where α, h, and v are the absorbance, Planck constant, and photon frequency [4]. The E_g was determined by extrapolation the linear portion of the curves to $(\alpha hv)^2 = 0$, corresponding to 2.47 eV and 2.36 eV for 120 min and 140 min, respectively. Indicate to, the interaction

between the lattice phonons and the free electrons and holes will also affect the band gap to a smaller extent. The relationship between band gap energy and temperature can be described by Varshni's empirical expression as show in equation (2.1),

$$E_g(T) = E_g(0) - \frac{\alpha T^2}{(T+\beta)}$$

It should be noted that the change of absorption was controlled by two photon energy ranges – the high and low energies. When the photon energy is greater than E_g, absorption was linearly increased with the increasing of photon energy. But for the photon energy of less than E_g, the absorption became different from the linearity, due to the dominant photonic absorption relating to defect levels between the valence and conduction bands of the products.
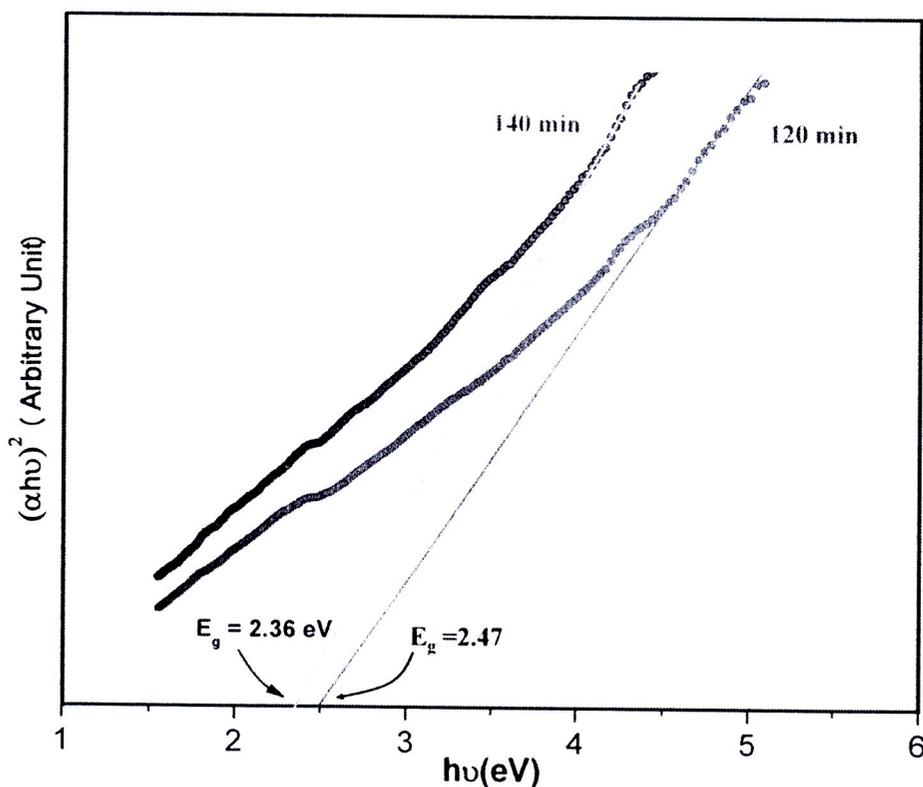

Figure 4.7 The $(\alpha h v)^2$ versus hv plots of CdS synthesized by the solid state microwave-plasma for 120 and 140 min
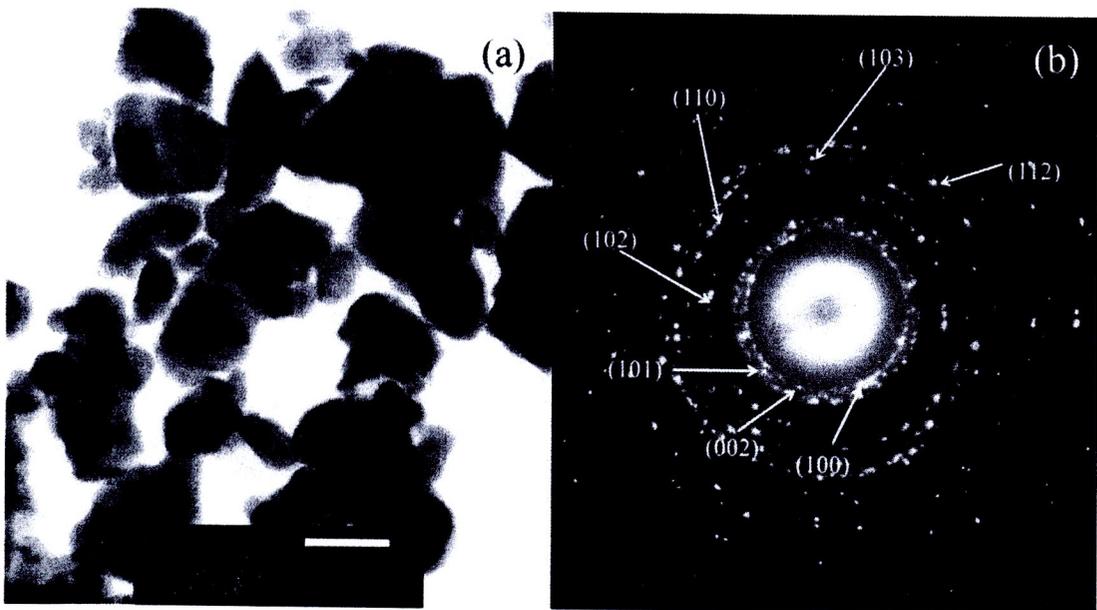
Figure 4.8 TEM image (a), and SAED pattern(b) of 1:2 molar ratio CdS produced for 100 min.

Table 4.9 Ring diffraction pattern values of 1:2 molar ratio CdS produced for 100 min, and the parameters of the JCPDS standard.

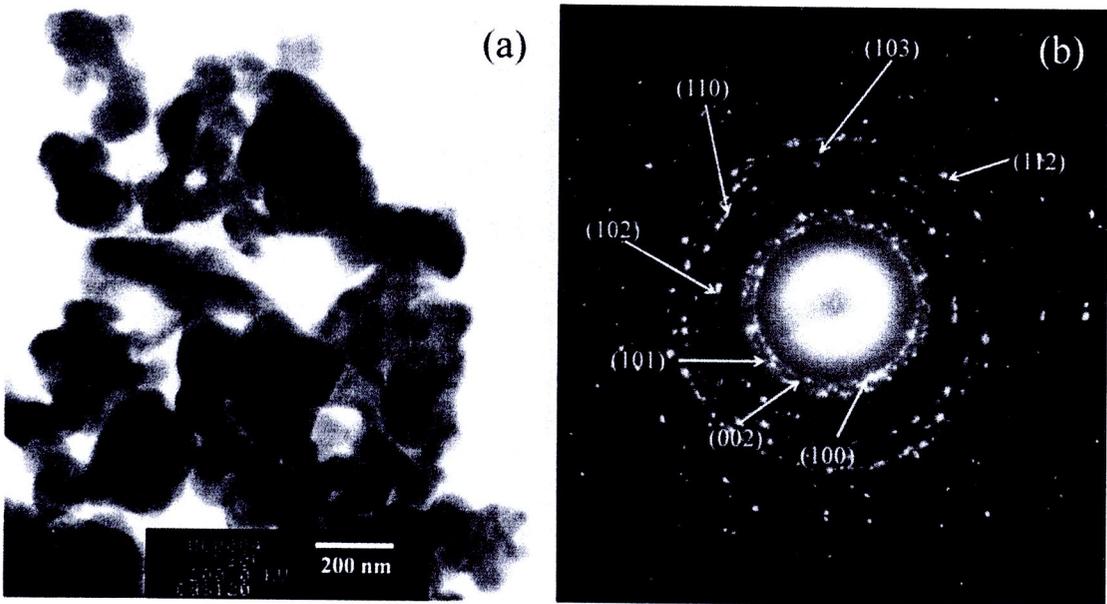| Ring No.	Diameter (mm)	Radius, R,(mm)	$d = L\lambda/R$ (^{o}A) (calculated)	d (^{o}A) (JCPDS file No.06-0314)	(hkl)
1	13.85	6.925	3.6048	3.583	100
2	14.86	7.43	3.3598	3.367	002
3	16.02	8.01	3.1165	3.160	101
4	20.5	10.25	2.4354	2.450	102
5	24.14	12.07	2.0682	2.068	110
6	26.16	13.08	1.9085	1.898	103

Figure 4.9 TEM image (a), and SAED pattern (b) of 1:2 molar ratio CdS produced for 120 min.

Table 4.10 Ring diffraction pattern values of 1:2 molar ratio CdS produced for 120 min, and the parameters of the JCPDS standard.

Ring No.	Diameter (mm)	Radius, R,(mm)	$d = L\lambda/R$ (^{o}A) (calculated)	d (^{o}A) (JCPDS file No.06-0314)	(hkl)
1	13.8	6.90	3.6178	3.583	100
2	14.7	7.35	3.3963	3.367	002
3	15.96	7.98	3.1282	3.160	101
4	20.42	10.21	2.4450	2.450	102
5	24.08	12.04	2.0733	2.068	110
6	26.26	13.13	1.9012	1.898	103

TEM image and SAED pattern of 1:2 molar ratio CdS products prepared by the microwave plasma for 100, 120 min shown in Figure 4.8 - 4.9, that the products was composed of irregular clusters of particles. The SAED patterns appear as bright spots arranging in concentric rings. These signify that the products are polycrystalline. Comparing the calculated interplanar spaces [33] to those of the JCPDS [78], CdS with hexagonal wultzite structure was identified. The ED patterns correspond to (100), (002), (101), (102), (110), (103) and (112) planes of the hexagonal wultzite CdS. These results accord closely with those of the XRD.

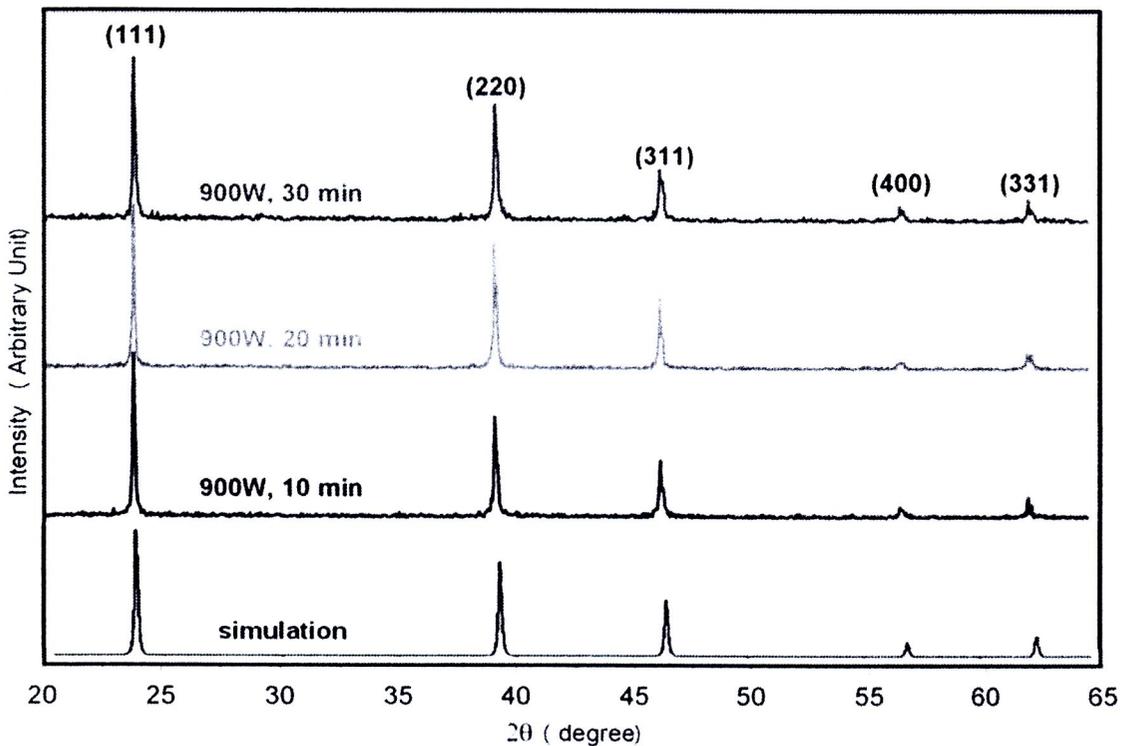## 4.2. CdTe synthesized by a microwave plasma technique

Figure 4.10 XRD patterns of CdTe synthesized using different 1:1(Cd:Te) molar ratios for 10, 20 and 30 min

X-ray diffraction patterns can provide an effective method for determining the phase and crystallite size of the CdTe samples. The XRD patterns of CdTe microstructure synthesized by microwave plasma technique are shown in Figure 4.10

XRD spectra of the products synthesized for different lengths of time are shown in Figure 4.10. The XRD spectra were interpreted as CdTe cubic structure with F-43m space group, comparing to the JCPDS database no 15-0770 [78]. Their diffraction peaks corresponding to the (111), (220), (311), (400), and (331) planes are at 2θ = 23.83, 39.38, 46.51, 56.92, and 62.50 deg, respectively for 10 min. By increasing the length of time to 30 min, the product's crystalline degree was the highest as show in Table 4.17. The reactants have more chance to form new product (CdTe), and the atoms have more chance to arrange themselves in their crystal lattices. Its lattice parameter (a) was calculated using Bragg's law for diffraction and the plane-spacing equation for cubic structure [7-9], and is summarized in Table 4.13 This parameter is 6.496±0.020 A°, which is very close to that of the JCPDS database no 15-0770 (a = 6.481 A°) - confirming the detection of cubic lattice structured CdTe.

An XRD diffraction pattern of CdTe was also simulated using the CaRIne program [79] in combination with the calculated lattice parameter, and is shown in Fig. 1. The 2θ Bragg's angles and diffraction intensities of different peaks of the experiment, simulation and JCPDS database no 15-0770 [78] are shown in Table 1. Both 2θ Bragg's angles and diffraction intensities of different peaks obtained from the experiment, simulation and JCPDS database are in good accordance.

Table 4.11 Calculated lattice parameter of CdTe from the experiment (molar ratio of Cd:Te=1:1, 10 min), comparing with the JCPDS file (Reference code: 15-0770 [78])

Plane	2θ (Exp.)	2θ (JCPDS)	d-spacing JCPDS A°	Lattice parameter (Exp.) A°	Lattice parameter (JCPDS) A°
(111)	23.83	23.759	3.742	6.4569	6.481
(220)	39.38	39.312	2.290	6.4664	6.481
(311)	46.51	46.434	1.954	6.4707	6.481
(400)	56.92	56.821	1.619	6.4657	6.481
(331)	62.50	62.353	1.488	6.4723	6.481
			Average.	6.4664±0.006	6.481

Table 4.12 Calculated lattice parameter of CdTe from the experiment (molar ratio of Cd:Te=1:1, 20 min), comparing with the JCPDS file (Reference code: 15-0770 [78])

Plane	2θ (Exp.)	2θ (JCPDS)	d-spacing JCPDS A°	Lattice parameter (Exp.) A°	Lattice parameter (JCPDS) A°
(111)	23.84	23.759	3.742	6.4596	6.481
(220)	39.37	39.312	2.290	6.4680	6.481
(311)	46.48	46.434	1.954	6.4747	6.481
(400)	56.91	56.821	1.619	6.4668	6.481
(331)	62.53	62.353	1.488	6.4695	6.481
			Average.	6.4677±0.005	6.481

Table 4.13 Calculated lattice parameter of CdTe from the experiment (molar ratio of Cd:Te=1:1, 30 min), comparing with the JCPDS file (Reference code: 15-0770 [78])

Plane	2θ (Exp.)	2θ (JCPDS)	d-spacing JCPDS A°	Lattice parameter (Exp.) A°	Lattice parameter (JCPDS) A°
(111)	23.85	23.759	3.742	6.4569	6.481
(220)	39.40	39.312	2.290	6.4633	6.481
(311)	46.51	46.434	1.954	6.4707	6.481
(400)	56.91	56.821	1.619	6.4668	6.481
(331)	62.55	62.353	1.488	6.4677	6.481
			Average.	6.4650±0.005	6.481

Table 4.14 The 2θ diffraction angles and intensities of the JCPDS no. 15-0770 [78] of Cd:Te, 900W and 10 min product obtained from the experiment and simulation.

Plane (hkl)	JCPDS (no. 15-0770)		Experimental		Simulation	
	2θ (deg.)	Intensity (%)	2θ (deg.)	Intensity (%)	2θ (deg.)	Intensity (%)
(111)	23.759	100	23.83	100	23.76	100
(220)	39.312	60	39.38	55.06	39.29	75.3
(311)	46.434	30	46.51	34.77	46.43	44.7
(400)	56.821	6	56.92	5.64	56.77	11.4
(331)	62.353	10	62.50	8.5	62.41	16.4

Table 4.15 The 2θ diffraction angles and intensities of the JCPDS no. 15-0770 [78] of Cd:Te, 900W and 20 min product obtained from the experiment and simulation.

Plane (hkl)	JCPDS (no. 15-0770)		Experimental		Simulation	
	2θ (deg.)	Intensity (%)	2θ (deg.)	Intensity (%)	2θ (deg.)	Intensity (%)
(111)	23.759	100	23.84	100	23.76	100
(220)	39.312	60	39.37	72.27	39.29	75.3
(311)	46.434	30	46.48	44.89	46.43	44.7
(400)	56.821	6	56.91	3.78	56.77	11.4
(331)	62.353	10	62.53	6.49	62.41	16.4

Table 4.16 The 2θ diffraction angles and intensities of the JCPDS no. 15-0770 [78] of Cd:Te, 900W and 30 min product obtained from the experiment and simulation.

Plane (hkl)	JCPDS (no. 15-0770)		Experimental		Simulation	
	2θ (deg.)	Intensity (%)	2θ (deg.)	Intensity (%)	2θ (deg.)	Intensity (%)
(111)	23.759	100	23.85	100	23.76	100
(220)	39.312	60	39.40	63.12	39.29	75.3
(311)	46.434	30	46.51	24.34	46.43	44.7
(400)	56.821	6	56.91	6.88	56.77	11.4
(331)	62.353	10	62.55	7.21	62.41	16.4

Table 4.17 Crystallinities percentage of 1:1 molar ratio for 10, 20, 30 min and standard values.

Condition	Intensity (%) of peak (101)	Intensity (%) of peak (400)	Intensity ratio (111)/(400)
10 min	100	5.64	17.73
20 min	100	3.78	26.46
30 min	100	6.88	14.53
JCPDS	100	6	16.67
Simulation	100	11.4	8.77

Table 4.18 The crystallite size (D) of 1:2 molar ratio CdTe for 10, 20 and 30 min products calculated from the scherrer's formula and the full width at half maximum (FWHM) of the XRD spectra

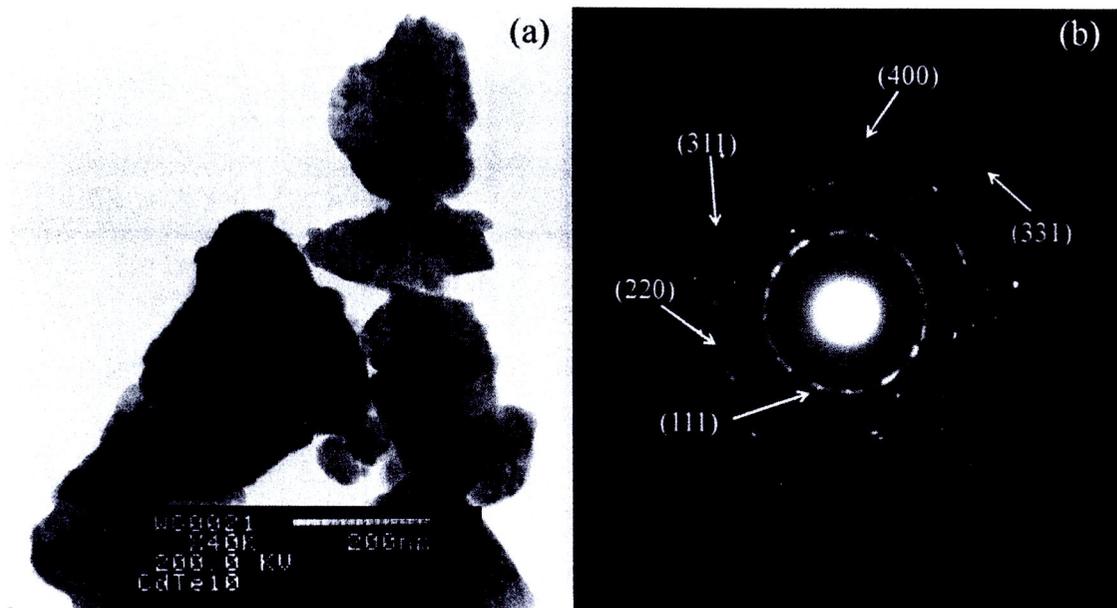| Experiment	Power heating	2θ	FWHM	D (nm)
10 min	900W	23.83	0.1574	51.583
20 min	900W	23.84	0.1574	51.584
30 min	900W	23.85	0.1574	51.585

Figure 4.11 TEM images (a) and ED patterns (b) of CdTe synthesized via the 900W microwave plasma for 10 min.

Table 4.19 Ring diffraction pattern values of 1:1 molar ratio CdTe produced for 10 min, and the parameters of the JCPDS standard.

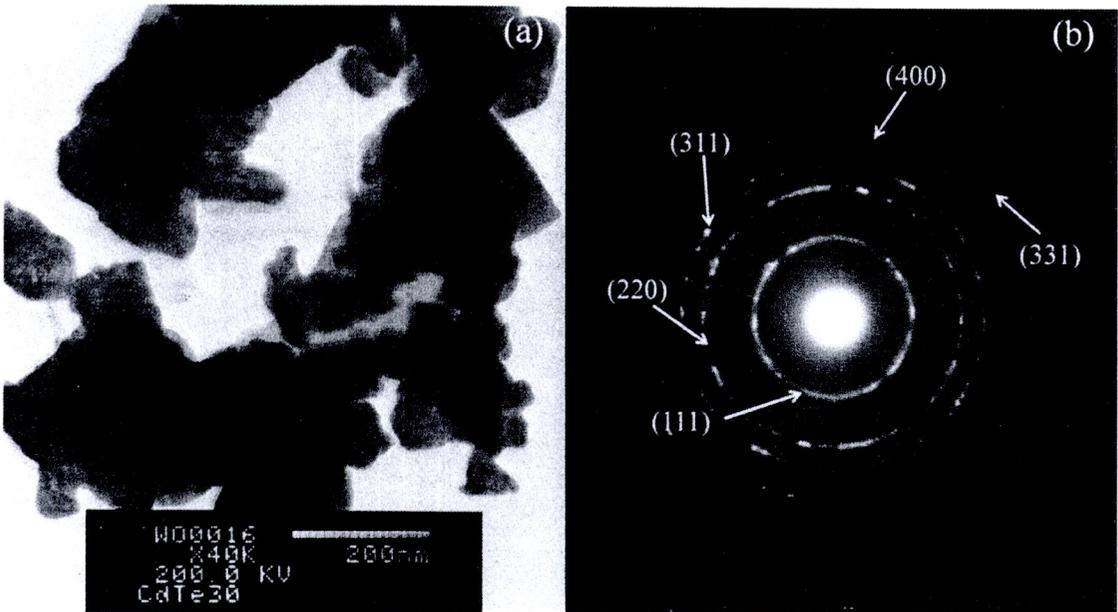| Ring No.	Diameter (mm)	Radius, R,(mm)	$d = L\lambda/R$ ($^{\circ}$A) (calculated)	d ($^{\circ}$A) (JCPDS file) No. 15-0770)	(hkl)
1	13.30	6.65	3.7538	3.74	111
2	21.78	10.89	2.2923	2.29	220
3	25.48	12.74	1.9594	1.95	311
4	30.88	15.44	1.6168	1.62	400
5	33.58	16.79	1.4868	1.48	331
6	37.60	18.80	1.3278	1.32	422

Figure 4.12 TEM images (a) and ED patterns (b) of CdTe synthesized via the 900W microwave plasma for 30 min.

Table 4.20 Ring diffraction pattern values of 1:1 molar ratio CdTe produced for 30 min, and the parameters of the JCPDS standard.

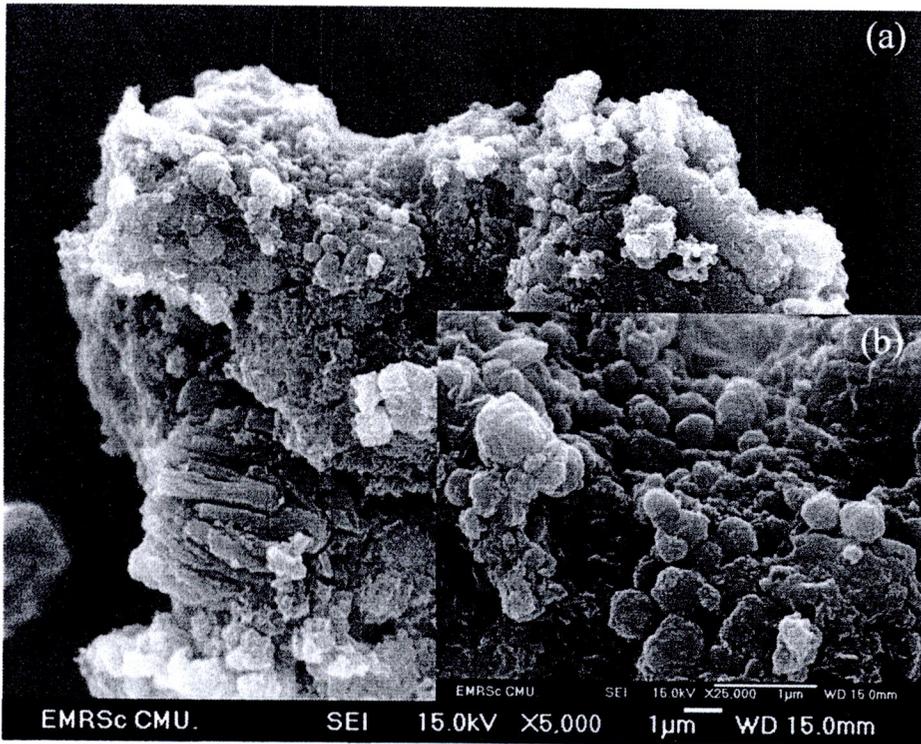| Ring No.	Diameter (mm)	Radius, R,(mm)	$d = L\lambda/R$ (^{o}A) (calculated)	d (^{o}A) (JCPDS file) No.15-0770)	(hkl)
1	13.32	6.66	3.7482	3.74	111
2	21.68	10.84	2.3029	2.29	220
3	25.36	12.68	1.9687	1.95	311
4	30.56	15.28	1.6337	1.62	400
5	33.3	16.65	1.4993	1.48	331
6	37.28	18.64	1.3392	1.32	422

Figure 4.13 SEM image and clusters sizes of 1:1 molar ratio CdTe product for 10 min
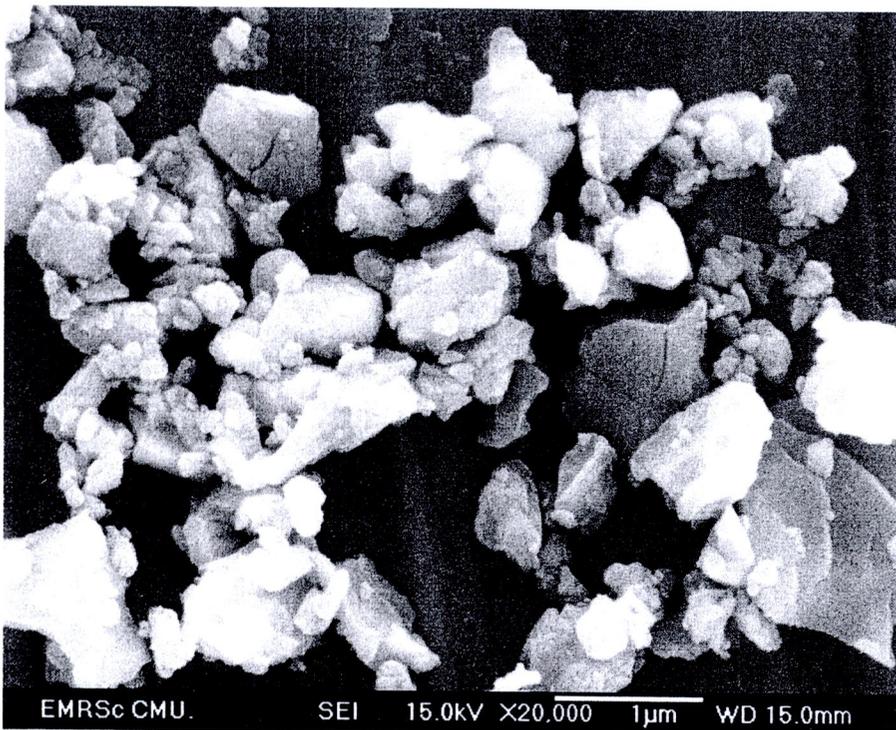

Figure 4.14 SEM image and clusters sizes of 1:1 molar ratio CdTe product for 20 min
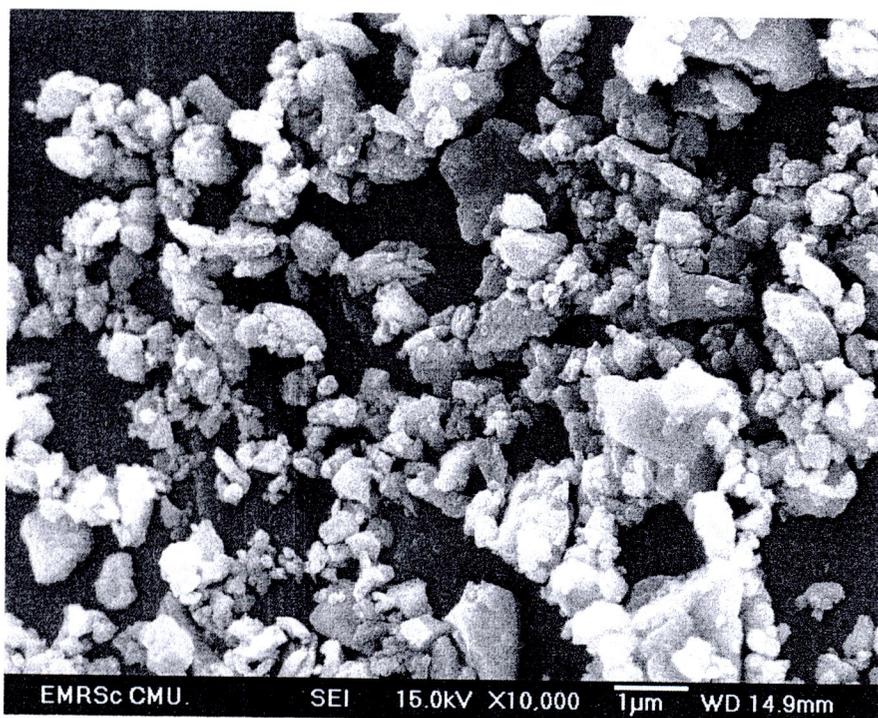
Figure 4.15 SEM image and clusters sizes of 1:1 molar ratio CdTe product for 30 min

Figure 4.11 - 4.12 shows SAED patterns of nanostructured CdTe synthesized by the 900 W microwave plasma for 10 and 30 min. The patterns appear as white concentric rings, characterized as polycrystals. These rings are diffuse and hollow showing that the product was composed of a number of nanosized crystals. At the present stage, the electron beam reflected and diffracted from polycrystals to form the concentric rings. Interplanar spaces (d) were calculated using their diffraction ring diameters [7-9], and compared with those of the JCPDS database no 15-0770 [78]. They both correspond to the (111), (220), (311), (400), and (331) crystallographic planes of the products and were specified as cubic CdTe.
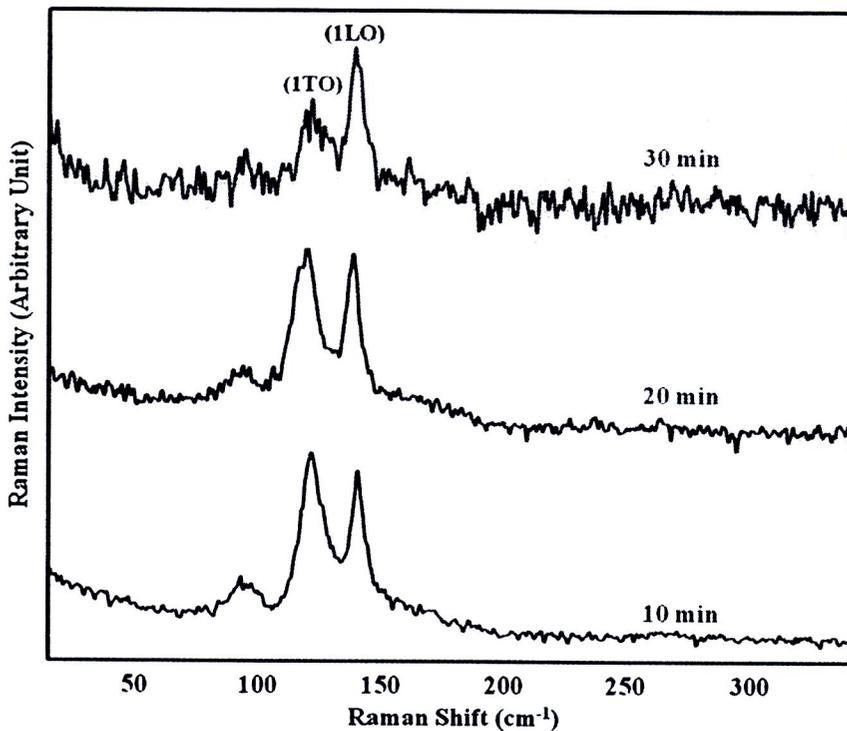
Figure 4.16 Raman spectra of CdTe synthesized under microwave power at 900 watt various the length of time for heating on 10, 20 and 30 min

The presence of cubic CdTe can be analyzed using a Raman spectrometer. For this case, test specimens are non-destructive and can be re-used for other purposes. The Raman shifts (Figure 4.16) show the vibration modes of CdTe, corresponding to the fundamental transverse optical (1TO) and longitudinal optical (1LO) vibrations at 140 cm^{-1} and 169 cm^{-1}, respectively. They are in good accordance with those obtained by Dutta et al. who specified the 1TO, and 1LO Raman shifts of CdTe at 141, and 166 cm^{-1} [21], and by Campos et al. at 141, and 167 cm^{-1} [22], respectively. Other peaks at 120 cm^{-1} were caused by the residual Te [22], although the Te peaks were not detected by XRD measurement – its concentration could be too low to be detected by the XRD analysis. By increasing the length of time, this 120 cm^{-1} peak became lower – implying that the Te content became lessened. It should be noted that the 140 cm^{-1}

peak was influenced not only by the vibration of cubic CdTe, but also the residual Te

[22]. Comparing to the XRD results, the 140 cm^{-1} peak was dominantly influenced by
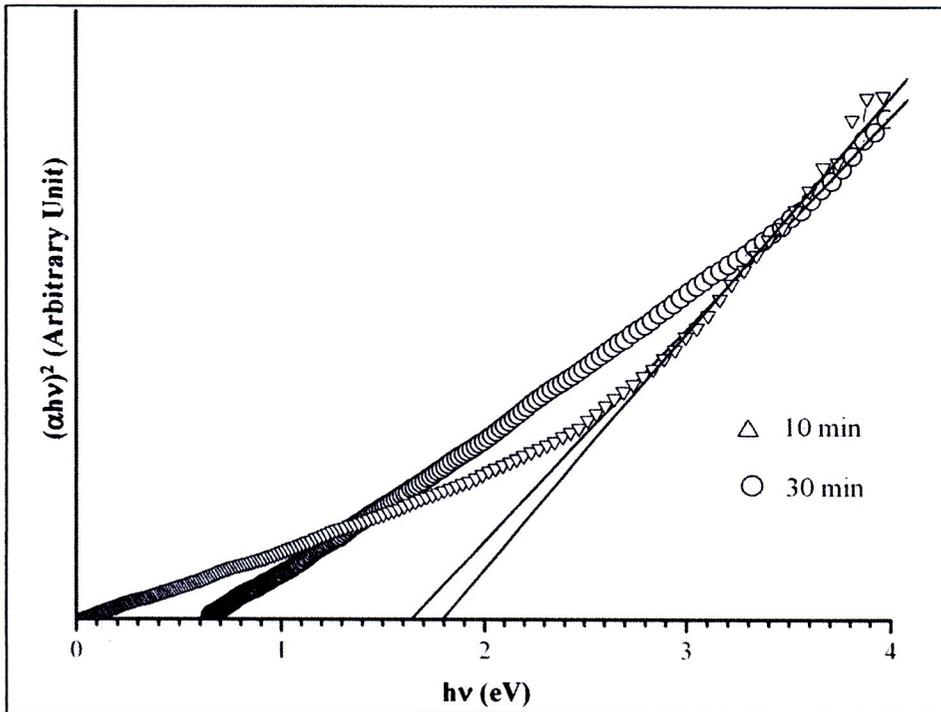
the vibration of nanostructured CdTe.

Figure 4.17 The $(\alpha h\nu)^2$ versus hν plots of CdTe synthesized under various of length of

time on 10 and 30 min

UV-vis absorbance of CdTe was recorded. The direct energy gap (E$_g$) was

determined by plotting $(\alpha h\nu)^2$ versus $h\nu$ (Figure 4.17). The energy band gap (E$_g$)

were determined by extrapolation the linear portion of the curves to $(\alpha h\nu)^2 = 0$,

corresponding to 1.80 eV and 1.65 eV for 10 min and 30 min, respectively. These

direct energy band gap are in accordance with as-deposited is 1.64 eV and annealed

CdTe films is 1.50 eV as determined by A.V. Kokate, M.R. Asabe [31], S.K. Pandey

[8] detected energy band gap by extrapolation curve of UV absorbance of cadmium

telluride thin films, which prepared by pulsed laser deposition (PLD) at 1.54 eV for hexagonal phase and about ~1.60 for cubic phase. It should be noted that the band gap of cubic CdTe for bulk is 1.5 eV at 300 K [17].

It should be noted that the change of absorption was controlled by two photon energy ranges – the high and low energies. When the photon energy is greater than E_g, absorption was linearly increased with the increasing of photon energy. But for the photon energy of less than E_g, the absorption became different from the linearity, due to the dominant photonic absorption relating to defect levels between the valence and conduction bands of the products.

4.3. ZnTe synthesized by a microwave plasma technique

X-ray diffraction patterns can provide an effective method for determining the phase and crystallite size of the ZnTe samples. The XRD patterns of ZnTe microstructure synthesized by microwave plasma technique are shown in Figure 4.18

The representative XRD patterns of the products are show in Figure 4.18. All spectra of the products were characterized using XRD and JCPDS database (Reference codes: 15-0746 for ZnTe, 01-1238 for Zn, and 01-0714 for Te) [78]. At 1:1 molar ratio of Zn:Te and under the 300, 450, 600 and 900 watt conditions, the products (300 and 450 watt) were composed of ZnTe with some impurities. For 300 watt, both Zn and Te impurities were left in the product. When the power heating was increased to 450 watt, only Te impurity was left in the main products. No such impurities were detected, when the experimental power was increased to 600 and 900 watt. At the present stage, the chemical reaction of Zn and Te was complete, and only cubic ZnTe was produced as the main product. The sharp peaks indicated good

crystallization of ZnTe. The strongest intensity peak is at $2\theta = 25.236$ degrees and diffracts from the (111) planes of the products.
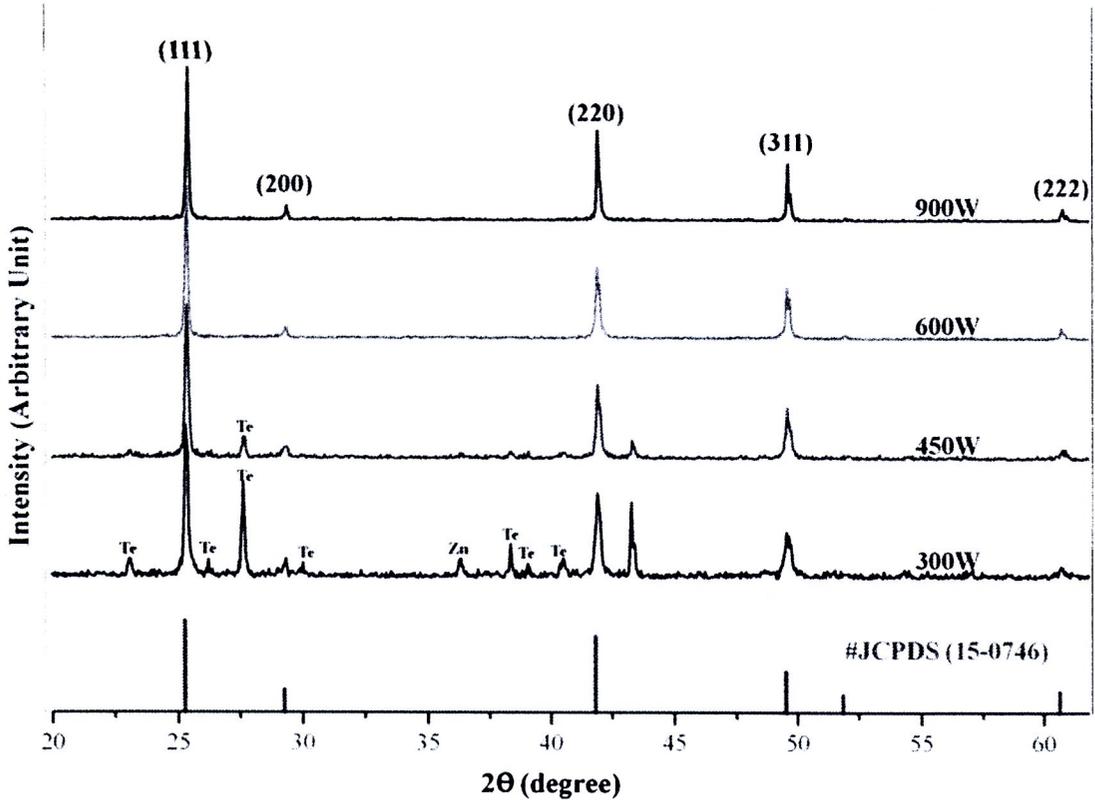

Figure 4.18 XRD patterns of ZnTe synthesized using different 1:1(Zn:Te) heating power for 300, 450, 600 and 900 W for 30 min.

The interplanar spacings (*d*) and lattice parameters (*a*) of different diffraction peaks of the 1:1 molar ratio Zn:Te product were calculated using Bragg's law for diffraction, and the plane-spacing equation for cubic structure [7-9]. These d spaces of different planes and average lattice parameter (*a* = 6.0992±0.0036Å, 6.1004±0.0041Å for 600 and 900 watt repectively) (Table 4.21- 4.22) are in good accordance with those of the JCPDS standard [78].

Table 4.21 Calculated lattice parameter of ZnTe from the experiment (molar ratio of Zn:Te = 1:1, 600 watt.) comparing with the JCPDS file (15-0746)

Plane	2θ, Exp. (deg.)	2θ, JCPDS file (deg.)	Interplanar spacing (d), (Exp.) Å	Interplanar Spacing (d) JCPDS file, Å	Lattice parameter, (Exp.)Å	Lattice parameter JCPDS file, Å
(111)	25.240	25.259	3.5243	3.5230	6.1042	6.1026
(200)	29.240	29.248	3.0506	3.0510	6.1012	6.1026
(220)	41.856	41.806	2.1557	2.1590	6.0972	6.1026
(311)	49.514	49.498	1.8387	1.8400	6.0984	6.1026
(222)	51.908	51.847	1.7594	1.7620	6.0948	6.1026

<div align="center">6.0992±0.0036</div>

Table 4.22 Calculated lattice parameter of ZnTe from the experiment (molar ratio of Zn:Te = 1:1, 900 watt.) comparing with the JCPDS file (15-0746)

Plane	2θ, Exp. (deg.)	2θ, JCPDS file (deg.)	Interplanar spacing (d), (Exp.) Å	Interplanar Spacing (d) JCPDS file, Å	Lattice parameter, (Exp.)Å	Lattice parameter JCPDS file, Å
(111)	25.236	25.259	3.5248	3.5230	6.1052	6.1026
(200)	29.230	29.248	3.0516	3.0510	6.1033	6.1026
(220)	41.868	41.806	2.1551	2.1590	6.0956	6.1026
(311)	49.528	49.498	1.8383	1.8400	6.0968	6.1026
(222)	51.85	51.847	1.7613	1.7620	6.1012	6.1026

<div align="center">6.1004±0.0041</div>

Table 4.23 The 2θ diffraction angles and intensities of the JCPDS no. 15-0746 [78] of Zn:Te, 600W for 30 min product obtained from the experiment and simulation.

Plane (hkl)	JCPDS (no. 15-0746)		Experimental		Simulation	
	2θ (deg.)	Intensity (%)	2θ (deg.)	Intensity (%)	2θ (deg.)	Intensity (%)
(111)	25.259	100	25.32	100	25.26	100
(200)	29.248	10	29.36	8.28	29.24	6.6
(220)	41.806	80	41.856	47.63	41.83	67.4
(311)	49.498	35	49.514	34.61	49.50	42.1
(222)	51.847	4	51.908	7.69	51.86	1.6

Table 4.24 The 2θ diffraction angles and intensities of the JCPDS no. 15-0746 [78] of Zn:Te, 900W for 30 min product obtained from the experiment and simulation.

Plane (hkl)	JCPDS (no. 15-0746)		Experimental		Simulation	
	2θ (deg.)	Intensity (%)	2θ (deg.)	Intensity (%)	2θ (deg.)	Intensity (%)
(111)	25.259	100	25.36	100	25.26	100
(200)	29.248	10	29.36	9.35	29.24	6.6
(220)	41.806	80	41.92	59.09	41.83	67.4
(311)	49.498	35	49.6	37.43	49.50	42.1
(222)	51.847	4	51.96	2.13	51.86	1.6

Table 4.25 The crystallite size (D) of 1:1 molar ratio ZnTe for 30 min products calculated from the scherrer's formula and the full width at half maximum (FWHM) of the XRD spectra

Experiment	2θ	FWHM	D (nm)
600 W	23.319	0.1574	51.729
900 W	25.362	0.1574	51.734

The average size which calculated using the Scherrer's equation are 51.729 nm for 600 W and 51.734 nm for 900 W. These values of average sizes were different from average size that was obtained from SEM image (figure 4.19-4.20) due to the average size were calculated form scherrer's equation were the average values of total particles but average size that was obtained from SEM image were cluster of nanostructure of the products. However, the average size of particle that calculated from scherrer's equation increase with the rising of power for synthesized because the thermal expansion of lattice.

SEM image and particle size distribution of the powder (Figure 4.19-4.20) showed that morphologies of the products prepared at 1:1 molar ratio of Zn:Te for 600 watt and 900 watt, it is composed of a number of nanoparticles in irregular clusters.
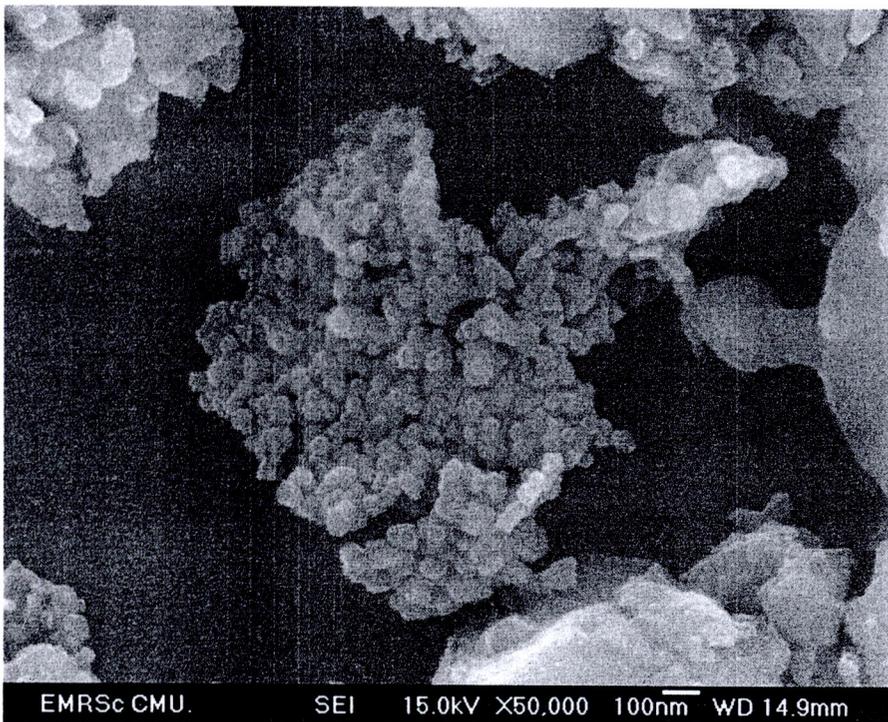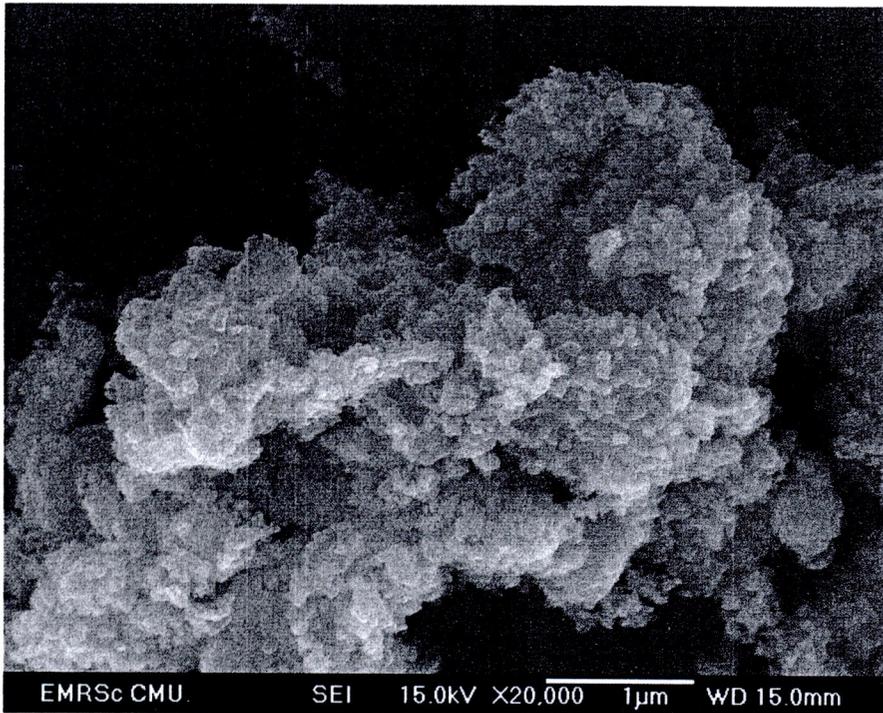
Figure 4.19 SEM image and clusters sizes of 600W and 1:1 molar ratio ZnTe product

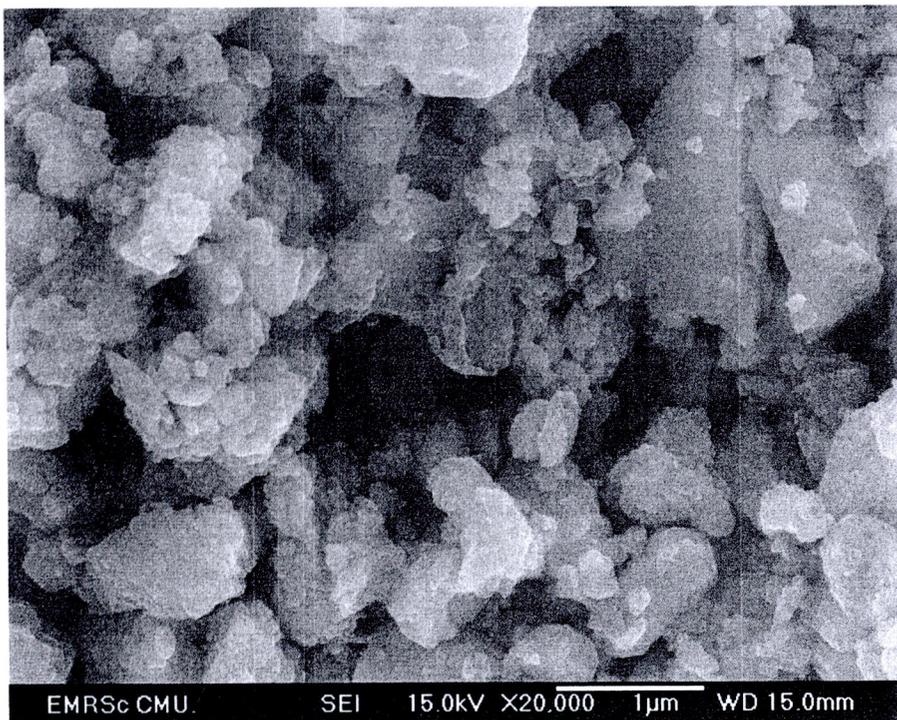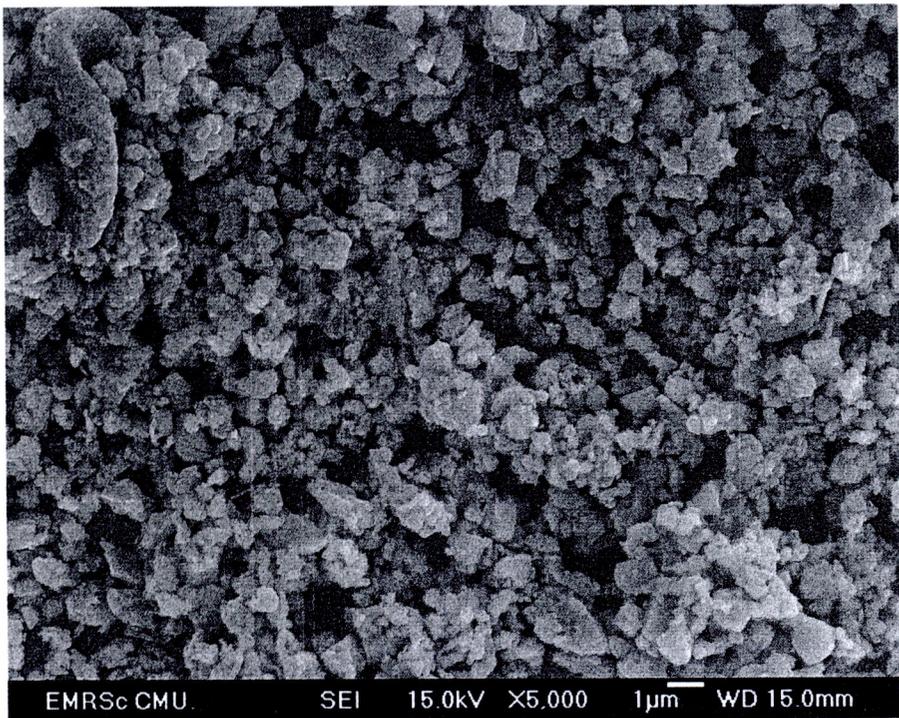for 30 min at x20,000 (a) x50,000 (b)

Figure 4.20 SEM image and clusters sizes of 900W and 1:1 molar ratio Zn:Te product

for 30 min at x5,000 (a) x20,000 (b)
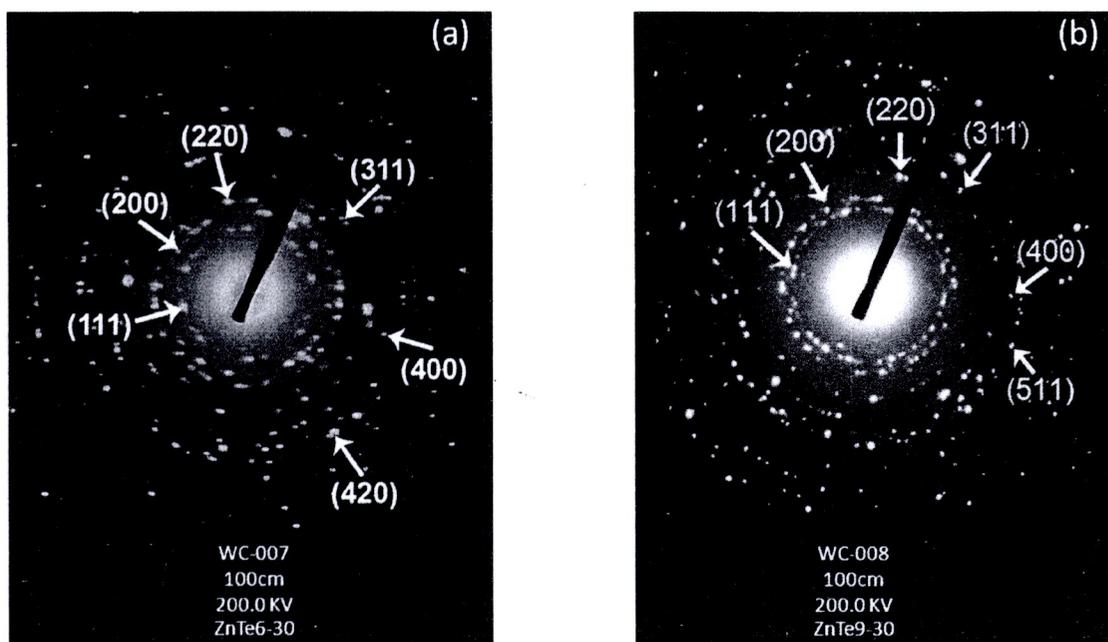
Figure4.21 SAED pattern of ZnTe produced under the 1:1 molar ratio of Zn:Te condition (a) 600 W (b) 900 W

Table4.26 Ring diffraction pattern values of ZnTe produced under the 1:1 molar ratio of Zn:Te, 600W and 30 min condition, and the parameters of the JCPDS standard.

Ring No.	Diameter (mm)	Radius, R,(mm)	$d = L\lambda/R$ (^{o}A) (calculated)	d (^{o}A) (JCPDS file No.15-0746)	(hkl)
1	14.2	7.10	3.51592	3.523	111
2	16.7	8.35	2.98958	3.051	200
3	23.7	11.85	2.10658	2.159	220
4	27.7	13.85	1.80238	1.840	311
5	33.2	16.60	1.50380	1.526	400
6	43.2	21.60	1.15569	1.1745	511

Table4.27 Ring diffraction pattern values of ZnTe produced under the 1:1 molar ratio of Zn:Te, 900W and 30 min condition, and the parameters of the JCPDS standard.

Ring No.	Diameter (mm)	Radius, R,(mm)	$d = L\lambda/R$ $(^{\circ}A)$ (calculated)	$d(^{\circ}A)$ (JCPDS file No.15-0746)	(hkl)
1	14.0	7.00	3.56614	3.523	111
2	17.0	8.50	2.93682	3.051	200
3	22.0	11.00	2.26936	2.159	220
4	26.0	13.00	1.92023	1.840	311
5	32.0	16.00	1.56019	1.526	400
6	36.0	18.00	1.38683	1.3645	420

SAED patterns of the products prepared by the microwave plasma are shown in Figures 4.21. The ZnTe products appeared as concentric rings of bright spots, showing that these products were composed of a number of nanocrystals with different orientations. The interplanarspacingswere calculated using diameters of the diffraction rings [7-9], and compared with those of the JCPDS standard [78]. The rings corresponded to the (111), (200), (220), (311), (400) and (511) planes of cubic ZnTe, produced under both the 600 W and 900 W of ZnTe conditions.
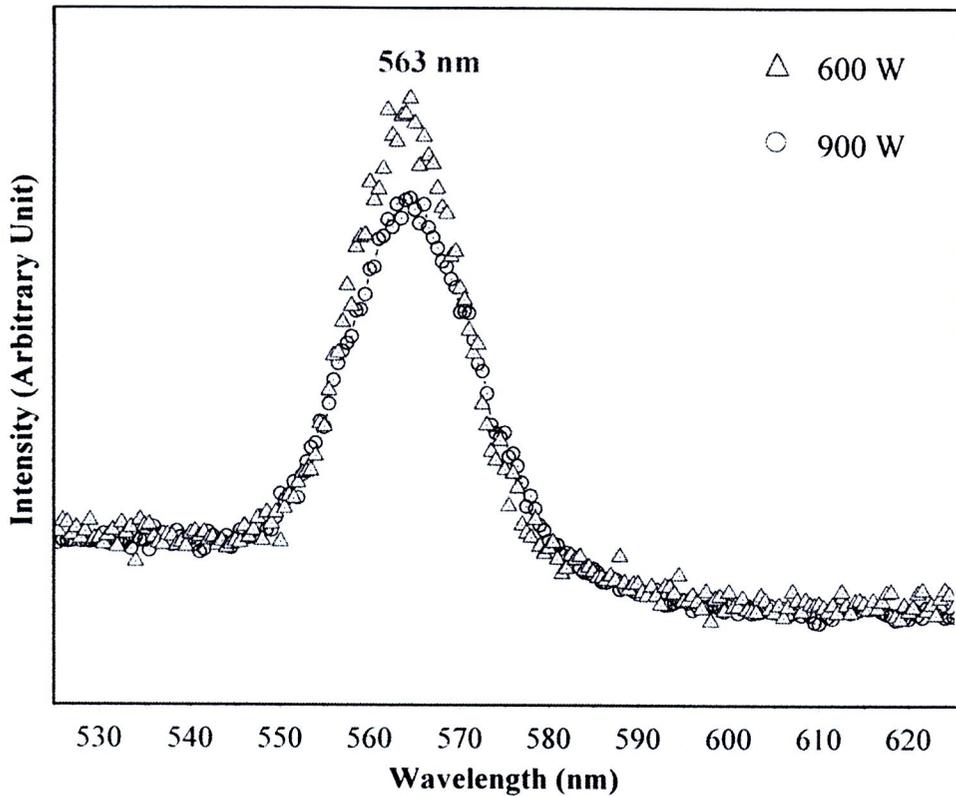
Figure 4.22 Photoluminescence of ZnTe produced under various of microwave power at 600 and 900 watt

Photoluminescence properties of cubic ZnTe were studied at room temperature, using 370 nm excitation wavelength from a Xenon laser. Their spectra (Figures 4.22) were green emission centered at around 563 nm (2.204 eV), possibly associated with point defects located at 0.46 eV above the valence band edge [6]. The emission were in accordance with those detected by Jiang et al (560 nm or 2.21 eV emitted from ZnTe nanowires) [51], and Park et al (552 nm or 2.25 eV) emitted from 14 nm nanocrystals) [76]. Comparing to ZnTe (bulk) with 2.26 eV band gap, the present emission has a slight red shift, which could be influenced by the twins in nanowires [51].

Comparing the emission of the 600 W and 900 W under same molar ratios of Zn:Te products, the intensities of 600 W is strongest than 900 W. Rate of reaction depend on temperature [72], therefore increasing of power heating has affected to increase the driving force of reaction, which promotes the reaction rate to become faster. For high reaction rate, atoms were arranged in the crystalline structure with low crystalline degree, which promoted the formation of some imperfections such as dislocations and other defects.
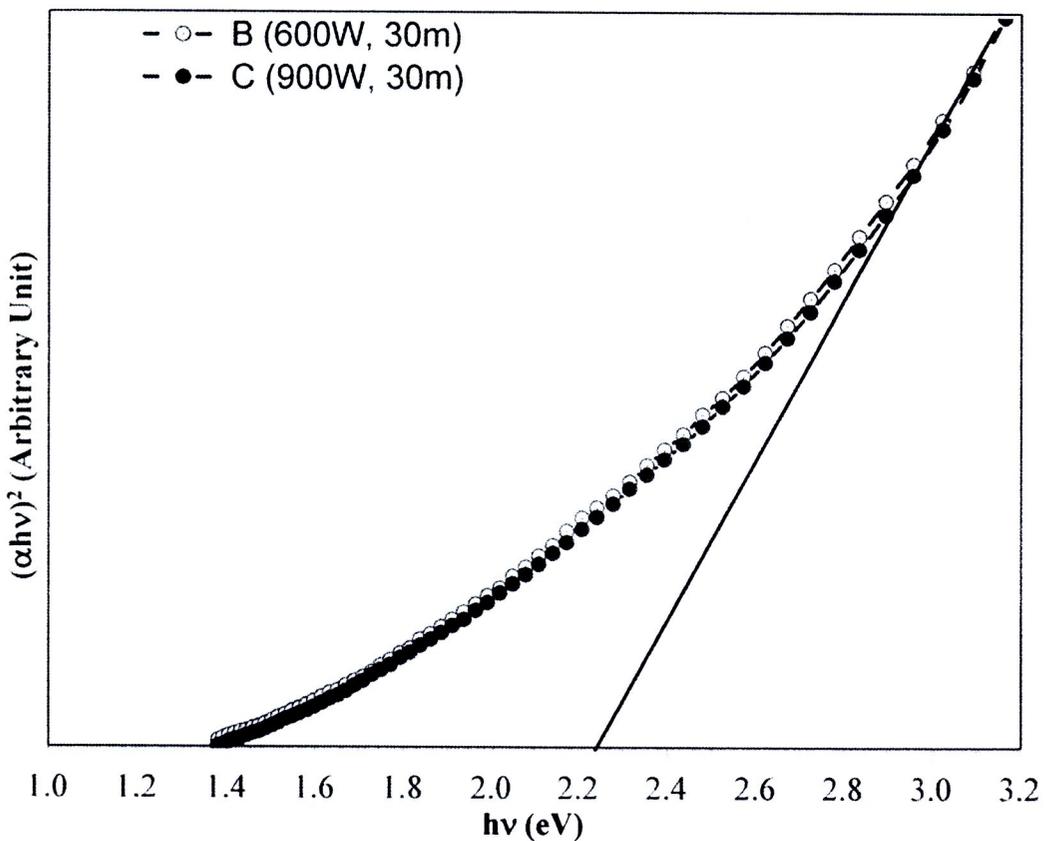

Figure 4.23 The $(\alpha h \nu)^2$ versus $h\nu$ plots of ZnTe synthesized under various of microwave power at 600 and 900 watt

UV-vis absorbance of ZnTe was recorded. The direct energy gap (E_g) was determined by plotting $(\alpha h \nu)^2$ versus $h\nu$ (Figure 4.23), where α, h, and ν are the

absorbance, Planck constant, and photon frequency [1]. The E_g was determined by extrapolation the linear portion of the curves to $(\alpha h v)^2 = 0$, corresponding to 2.24 eV. The data shown in Figure 4.22 and 4.23 illustrate the point that the emission (photoluminescence) and energy gap which determined by absorption spectra are not the same. The energy gap corresponds to the threshold for optical absorption, but photoluminescence peak will close and less than energy gap.
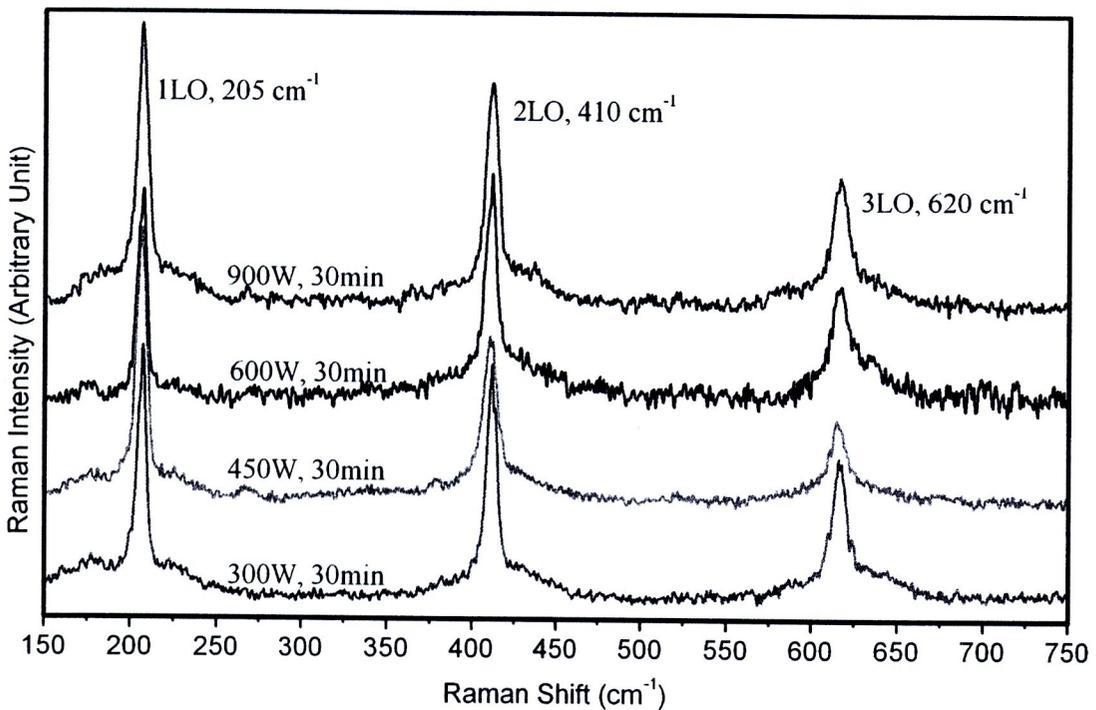
Figure 4.24 Raman spectra of ZnTe synthesized under various of microwave power at 300, 450, 600 and 900 watt

Figure 4.24 shows Raman spectra of cubic ZnTe nanocrystals, which were composed of three longitudinal optical (LO) modes of 1LO (1st harmonic or fundamental), 2LO (2nd harmonic or 1st overtone) and 3LO (3rd harmonic or 2nd overtone) at 205, 410, and 620 cm^{-1}, and one transverse optical (TO) mode at 166 cm^{-1}, respectively. These Raman shifts are in good accordance with those obtained by

Jiang et al. [51], who specified the 1LO, 2LO and TO Raman shifts of ZnTe nanowires at 198, 396 and 168 cm^{-1}, respectively. Comparing to 30 mW He-Ne laser with 632.8 nm (red) wave length, a great deal of energy was lost during the Raman analysis, due to the inelastic scattering process.

Figure 4.25 SEM images 600 W (a) 900 W (b) SAED patterns of ZnTe synthesized via the 900W microwave plasma for 30 min (c) simulation

4.4 ZnO film on FTO for DSSC synthesized by a microwave plasma technique
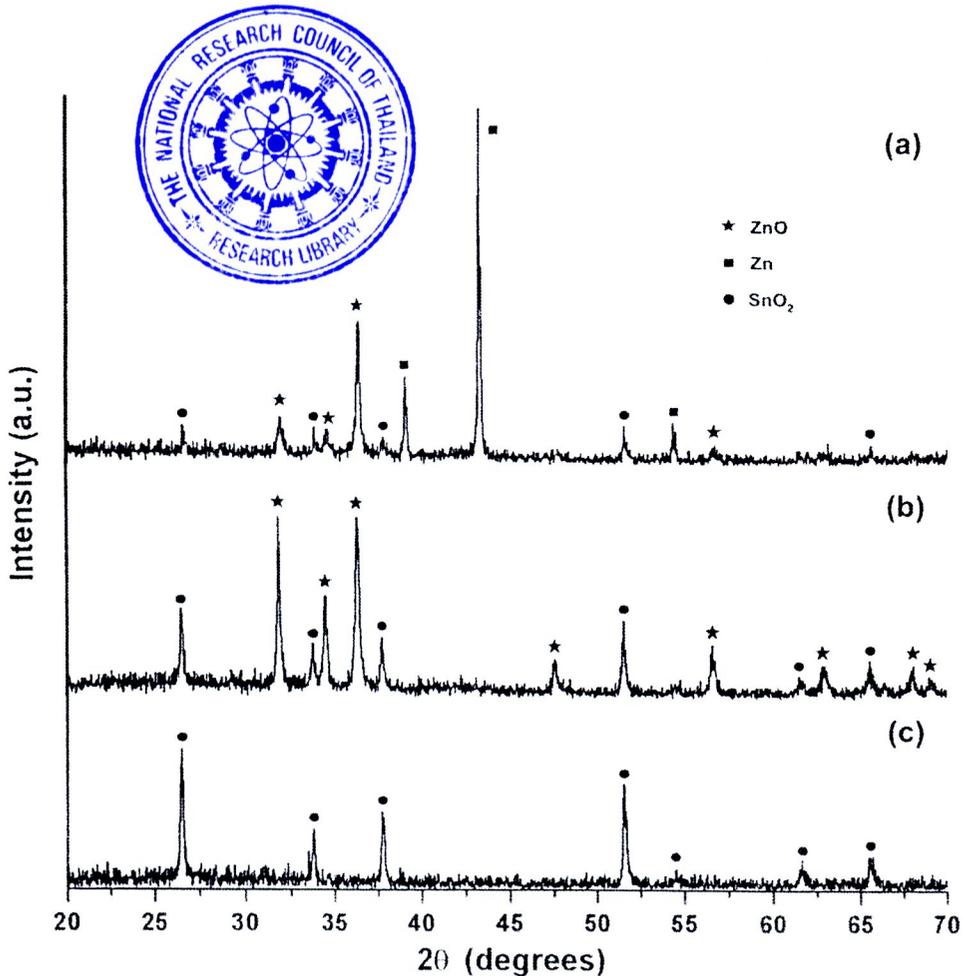
Figure 4.26 XRD patterns of (a) deposit ZnO thin film on FTO, (b) calcinations of porous Zn film to porous ZnO film, (c) FTO

The ZnO powder (5g) was synthesized according to the microwave plasma method mix with triton-X (10 ml) and stir by rotating magnet on stove that have the temperature at 75°C for 25 min. Afterward, the thick film of ZnO prepare via doctor-blade on substrates (FTO). The resulting substrates were heated in an oven at 400°C for 2h with a heating rate of 2°C/min and cooled down to room temperature with the heating rate of 2°C/min.

Figure 4.26 (a-c) shows XRD patterns of FTO glass and heat-treat film by microwave plasma of as-deposited Zn and calcinations of Zn to ZnO film on FTO glass. XRD pattern of as-deposited film can be referred to JCPDS standard (77-0452 for SnO_2, 04-0831 for Zn and 89-0511 for ZnO). All the peaks of ZnO particle, which deposited on film, were corresponds as hexagonal wurtzite structure (a=b=0.3249 nm and c=0.5205 nm) from the "orientation attrachment" theory proposed by Guang Zhu et al. [83].
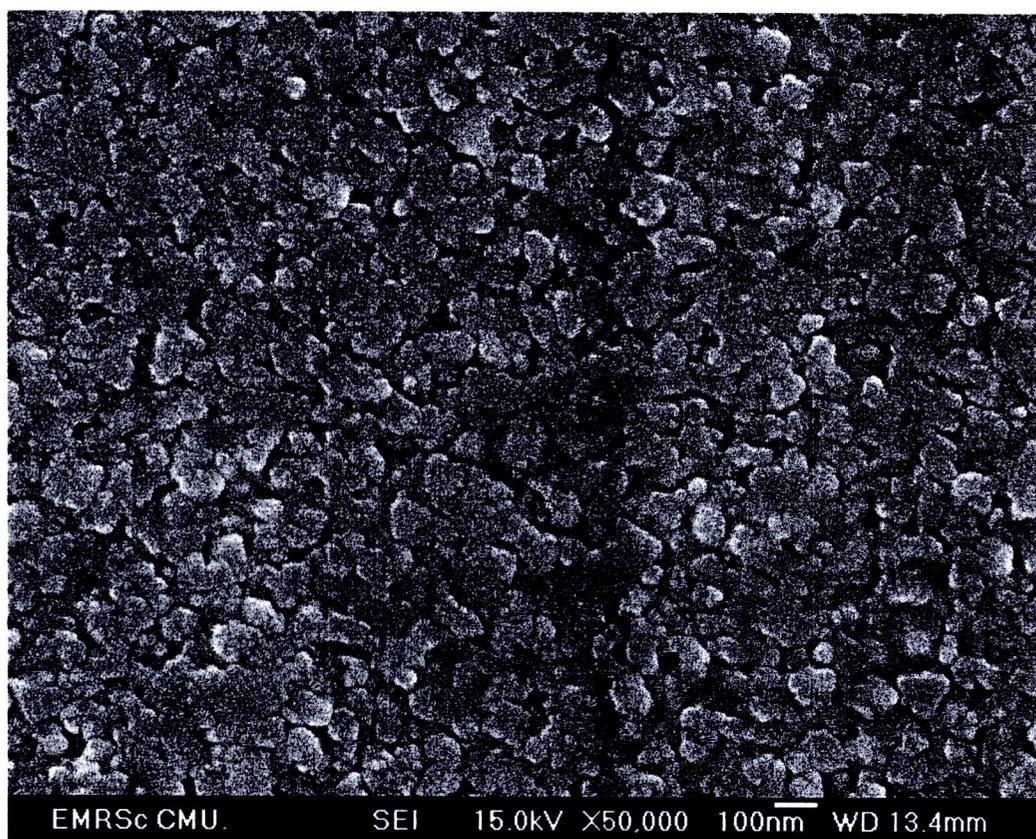

Figure 4.27 FE-SEM image of ZnO particles that deposited on FTO

FE-SEM image of the prepared ZnO film on FTO substrates in Figure 4.27 is composed of agglomerate particles with an average diameter of 100 nm.

4.5 CdTe-GPE composited electrolyte on quasi solid-state ZnO Based Dye Sensitized Solar Cells

From previous reports, ZnO were synthesized by microwave plasma (and sonochemical technique show in appendix A). These products were prepared on the FTO substrate via doctor-blade method [14] for perform photoelectrode. The gel polymer composite electrolyte preparation show that in Figure 4.28

```
┌─────────────────────────────────────────────────┐
│   LiI (0.5mM) : I (0.05mM) PEG20,000 (0.15mM)    │
│                        +                         │
│        Acetone nittrile (CH₃CN) (10ml)           │
└─────────────────────────────────────────────────┘
                         │
                         ▼
┌─────────────────────────────────────────────────┐
│                      Add                         │
│      p-CdTe with 0, 0.05, 0.15 and 0.20 %wt      │
└─────────────────────────────────────────────────┘
                         │
                         ▼
┌─────────────────────────────────────────────────┐
│      Stirring and heat at 60°C for 30 min till   │
│        clear and homogeneous quasi-solid state   │
└─────────────────────────────────────────────────┘
                         │
                         ▼
┌─────────────────────────────────────────────────┐
│            Polymer Electrolyte for               │
│                    DSSCs                          │
└─────────────────────────────────────────────────┘
```
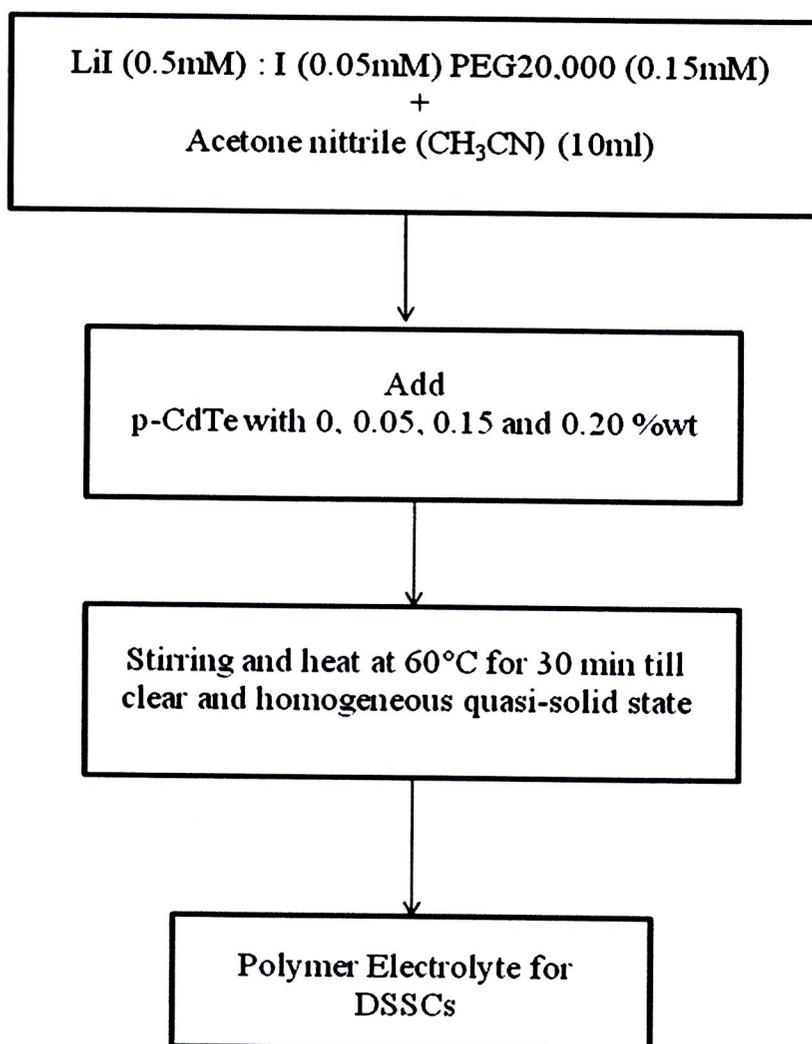
Figure 4.28 the flow chart for preparation the p-CdTe gel polymer composite electrolyte
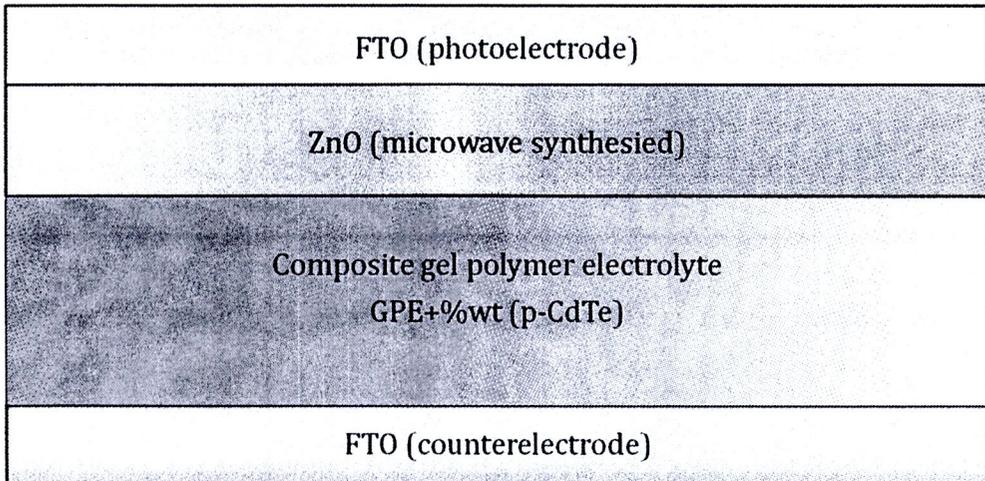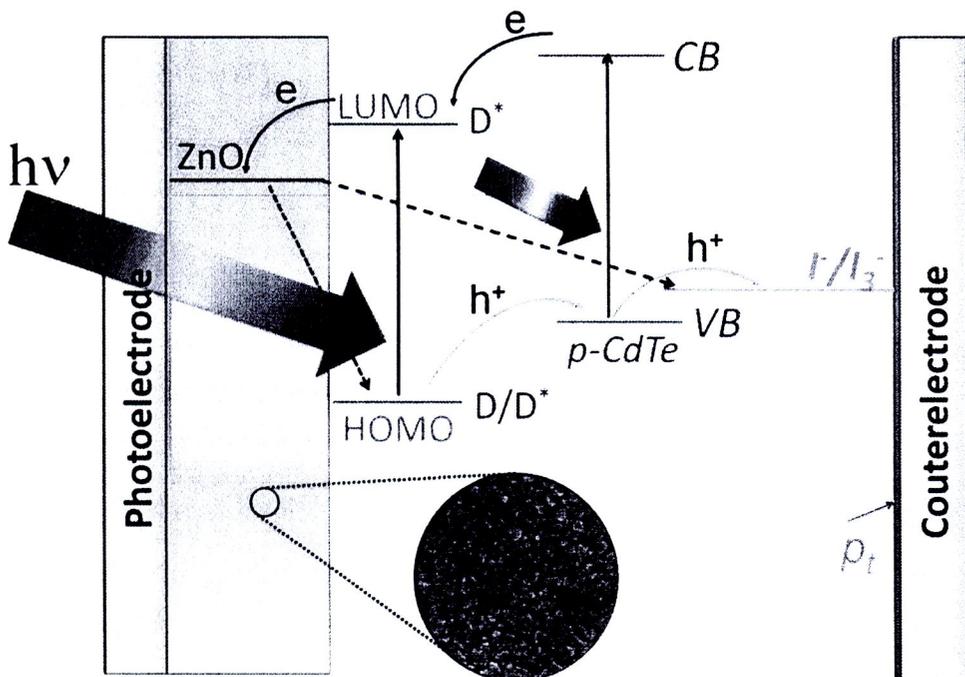
Figure 4.29 A schematic diagram of the CdTe-GPE-DSSCs

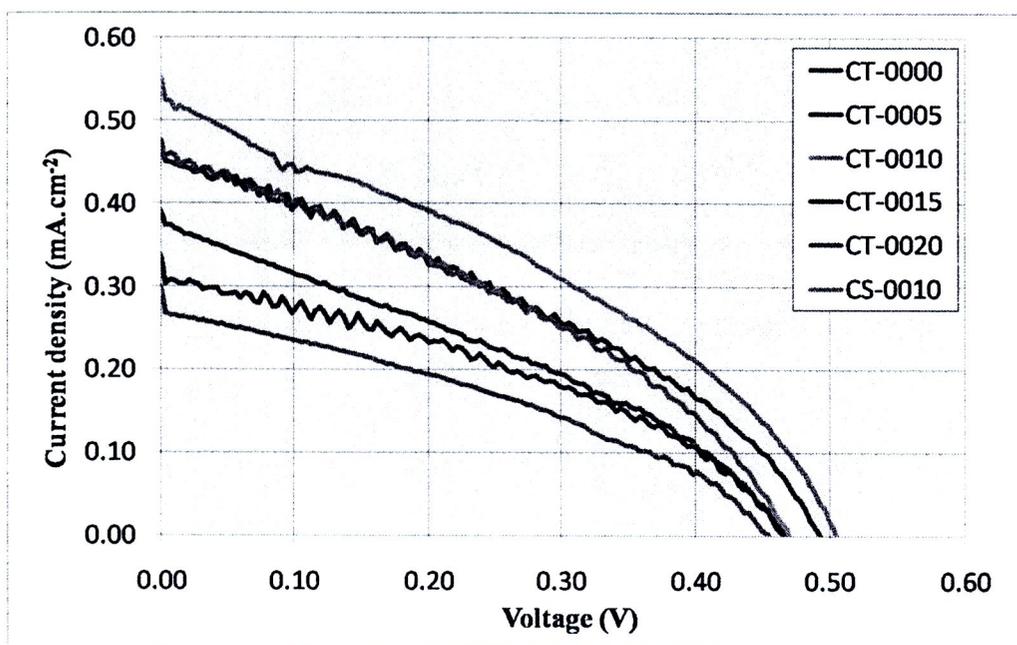Figure 4.30 the simplified energy level diagram of the CdTe-GPE-DSSCs

Figure 4.31 J-V characteristic curves of DSSCs for different wt % CdTe-GPE electrolyte.

Table 4.28 V_{oc}, J_{sc}, ff and η for different wt% CdTe-GPE

Samples	Electrolyte	J_{sc} (mA.cm^{-2})	V_{oc} (V)	ff	η (%)
CT-0000	GPE	0.389	0.468	0.322	0.058
CT-0005	0.05wt%CdTe-GPE	0.475	0.493	0.337	0.080
CT-0010	0.10wt%CdTe-GPE	0.551	0.504	0.337	0.093
CT-0015	0.15wt%CdTe-GPE	0.336	0.468	0.348	0.055
CT-0020	0.20wt%CdTe-GPE	0.298	0.455	0.321	0.044
CS-0010	0.10wt%CdS-GPE	0.471	0.468	0.348	0.077

In earliest stage, the efficiency of DSSC which add CdTe into gel polymer electrolyte increase with percentage by weight of CdTe, that it has efficiency highest at 0.093 % for 0.10% wt show that in table 4.28. Afterward, the efficiency of DSSCs

will be decrease when add CdTe 0.15 and 0.20% wt. For CdS (CS-0010) mix in gel polymer electrolyte at the same amount of percentage (0.10%wt), it was found that efficiency is lower than CdTe-GPE DSSC.

4.6 ZnTe-GPE composited electrolyte on quasi solid-state ZnO Based Dye Sensitized Solar Cells

From previous reports, ZnO were synthesized by microwave plasma. These products were prepared on the FTO substrate via doctor-blade method [14] for perform photoelectrode. The gel polymer composite electrolyte preparation show that in Figure 4.32
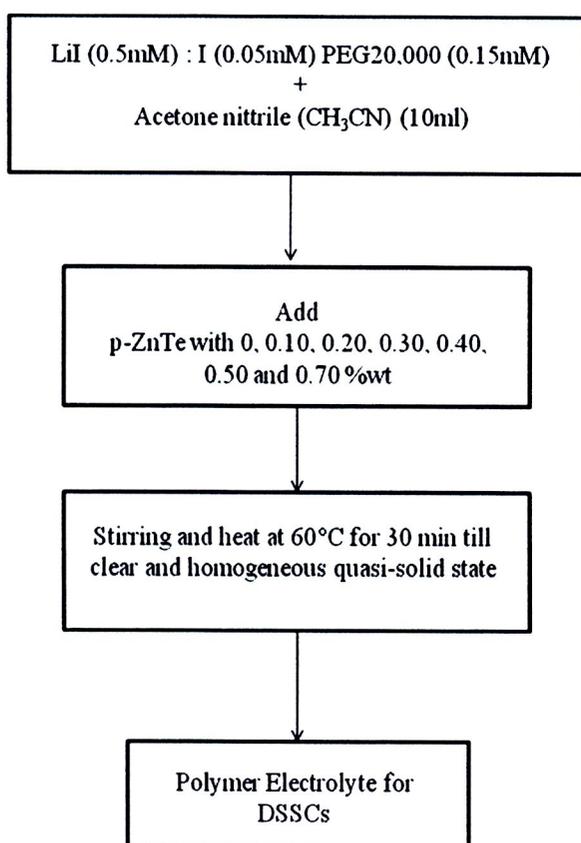
```
┌─────────────────────────────────────────────┐
│   LiI (0.5mM) : I (0.05mM) PEG20,000 (0.15mM) │
│                      +                         │
│       Acetone nittrile (CH₃CN) (10ml)         │
└─────────────────────────────────────────────┘
                        │
                        ▼
┌─────────────────────────────────────────────┐
│                    Add                         │
│   p-ZnTe with 0, 0.10, 0.20, 0.30, 0.40,      │
│            0.50 and 0.70 %wt                    │
└─────────────────────────────────────────────┘
                        │
                        ▼
┌─────────────────────────────────────────────┐
│   Stirring and heat at 60°C for 30 min till   │
│    clear and homogeneous quasi-solid state     │
└─────────────────────────────────────────────┘
                        │
                        ▼
┌─────────────────────────────────────────────┐
│            Polymer Electrolyte for             │
│                    DSSCs                        │
└─────────────────────────────────────────────┘
```

Figure 4.32 the flow chart for preparation the p-ZnTe gel polymer composite electrolyte

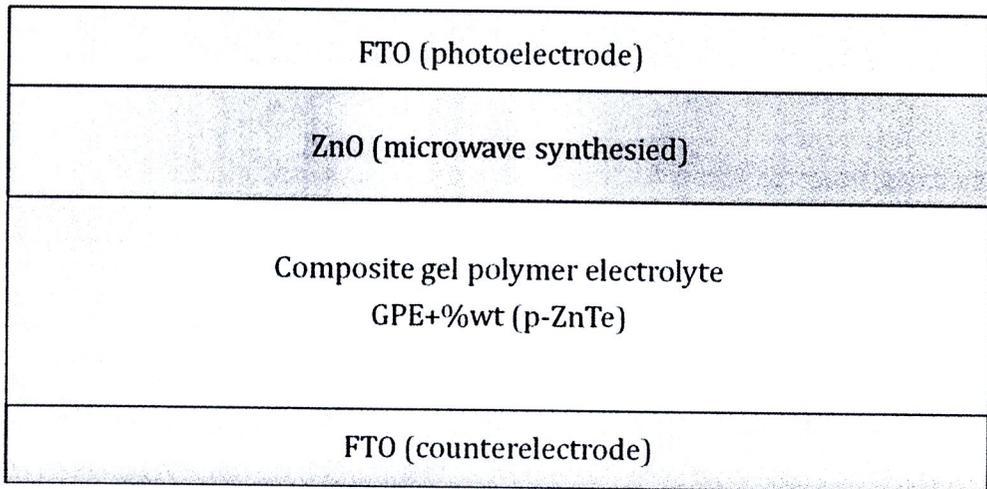| FTO (photoelectrode) |
|:---:|
| ZnO (microwave synthesied) |
| Composite gel polymer electrolyte
GPE+%wt (p-ZnTe) |
| FTO (counterelectrode) |

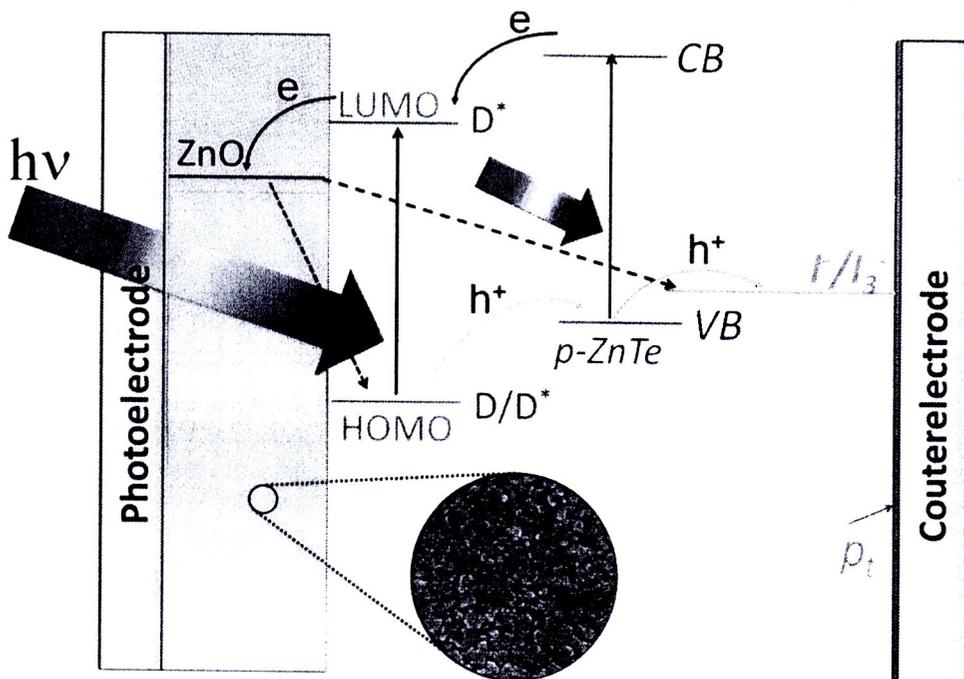Figure 4.33 A schematic diagram of the ZnTe-GPE-DSSCs

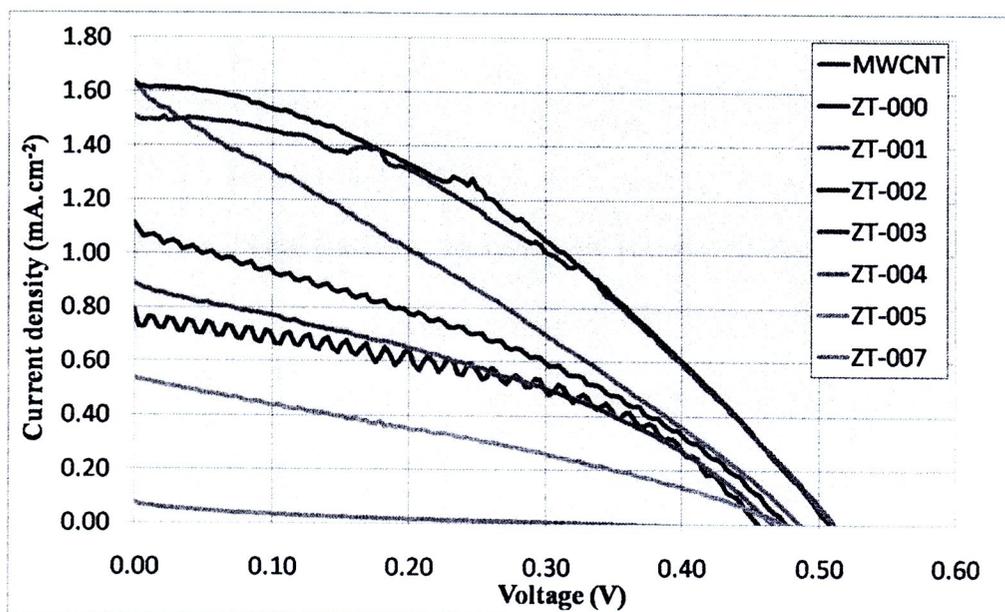Figure 4.34 the simplified energy level diagram of the ZnTe-GPE-DSSCs

Figure 4.35 J-V characteristic curves of DSSCs for different wt % CdTe-GPE electrolyte.

Table 4.29 V_{oc}, J_{sc}, ff and η for different wt% ZnTe-GPE

Samples	Electrolyte	J_{sc} (mA.cm^{-2})	V_{oc} (V)	ff	η (%)
MWCNT	GPE	0.788	0.455	0.444	0.159
ZT-000	GPE	1.113	0.476	0.343	0.182
ZT-001	0.10wt%ZnTe-GPE	1.631	0.487	0.274	0.218
ZT-002	0.20wt%ZnTe-GPE	1.635	0.508	0.383	0.318
ZT-003	0.30wt%ZnTe-GPE	1.510	0.512	0.402	0.310
ZT-004	0.40wt%ZnTe-GPE	0.893	0.465	0.363	0.151
ZT-005	0.50wt%ZnTe-GPE	0.539	0.476	0.306	0.078
ZT-007	0.70wt%ZnTe-GPE	0.0768	0.349	0.130	0.0035

In first stage, the efficiency of DSSCs which add ZnTe into gel polymer electrolyte increase with percentage by weight of ZnTe, that it has efficiency highest at 0.318 % for 0.20wt%ZnTe-GPE show that in table 4.29. Afterward, the efficiency of DSSCs will be decrease when add ZnTe 0.30, 0.40, 0.50 and 0.70% wt. In addition, the DSSCs with multi-wall carbon nanotube (MWCNT) counter electrode demonstrated nearby efficiency with using the platinum (Pt) counter electrode.